

NASA/TM—1998-208665

JN-26
43219/
42P



Modeling of Substitutional Site Preference in Ordered Intermetallic Alloys

Guillermo Bozzolo
Ohio Aerospace Institute, Cleveland, Ohio

Ronald D. Noebe and Frank Honey
Lewis Research Center, Cleveland, Ohio

The NASA STI Program Office . . . in Profile

Since its founding, NASA has been dedicated to the advancement of aeronautics and space science. The NASA Scientific and Technical Information (STI) Program Office plays a key part in helping NASA maintain this important role.

The NASA STI Program Office is operated by Langley Research Center, the Lead Center for NASA's scientific and technical information. The NASA STI Program Office provides access to the NASA STI Database, the largest collection of aeronautical and space science STI in the world. The Program Office is also NASA's institutional mechanism for disseminating the results of its research and development activities. These results are published by NASA in the NASA STI Report Series, which includes the following report types:

- **TECHNICAL PUBLICATION.** Reports of completed research or a major significant phase of research that present the results of NASA programs and include extensive data or theoretical analysis. Includes compilations of significant scientific and technical data and information deemed to be of continuing reference value. NASA's counterpart of peer-reviewed formal professional papers but has less stringent limitations on manuscript length and extent of graphic presentations.
- **TECHNICAL MEMORANDUM.** Scientific and technical findings that are preliminary or of specialized interest, e.g., quick release reports, working papers, and bibliographies that contain minimal annotation. Does not contain extensive analysis.
- **CONTRACTOR REPORT.** Scientific and technical findings by NASA-sponsored contractors and grantees.
- **CONFERENCE PUBLICATION.** Collected papers from scientific and technical conferences, symposia, seminars, or other meetings sponsored or cosponsored by NASA.
- **SPECIAL PUBLICATION.** Scientific, technical, or historical information from NASA programs, projects, and missions, often concerned with subjects having substantial public interest.
- **TECHNICAL TRANSLATION.** English-language translations of foreign scientific and technical material pertinent to NASA's mission.

Specialized services that complement the STI Program Office's diverse offerings include creating custom thesauri, building customized data bases, organizing and publishing research results . . . even providing videos.

For more information about the NASA STI Program Office, see the following:

- Access the NASA STI Program Home Page at <http://www.sti.nasa.gov>
- E-mail your question via the Internet to help@sti.nasa.gov
- Fax your question to the NASA Access Help Desk at (301) 621-0134
- Telephone the NASA Access Help Desk at (301) 621-0390
- Write to:
NASA Access Help Desk
NASA Center for AeroSpace Information
7121 Standard Drive
Hanover, MD 21076

NASA/TM—1998-208665



Modeling of Substitutional Site Preference in Ordered Intermetallic Alloys

Guillermo Bozzolo
Ohio Aerospace Institute, Cleveland, Ohio

Ronald D. Noebe and Frank Honeycy
Lewis Research Center, Cleveland, Ohio

Prepared for the
"Interstitial and Substitutional Effects in Intermetallics" Fall Meeting
sponsored by the Minerals, Metals, and Materials Society
Rosemont, Illinois, October 11-15, 1998

National Aeronautics and
Space Administration

Lewis Research Center

October 1998

Acknowledgments

Fruitful discussions with N. Bozzolo are gratefully acknowledged. We would also like to thank C. Amador for providing us with the first-principles input necessary for determining the BFS parameters used in this work.

Available from

NASA Center for Aerospace Information
7121 Standard Drive
Hanover, MD 21076
Price Code: A03

National Technical Information Service
5285 Port Royal Road
Springfield, VA 22100
Price Code: A03

MODELING OF SUBSTITUTIONAL SITE PREFERENCE IN ORDERED INTERMETALLIC ALLOYS

Guillermo Bozzolo^a, Ronald D. Noebe^b and Frank Honey^b

^aOhio Aerospace Institute, Cleveland, OH 44142, USA

^bNASA Lewis Research Center, Cleveland, OH 44135, USA.

Abstract

We investigate the site substitution scheme of specific alloying elements in ordered compounds and the dependence of site occupancy on compound stoichiometry, alloy concentration. This basic knowledge, and the interactions with other alloying additions are necessary in order to predict and understand the effect of various alloying schemes on the physical properties of a material, its response to various temperature treatments, and the resulting mechanical properties. Many theoretical methods can provide useful but limited insight in this area, since most techniques suffer from constraints in the type of elements and the crystallographic structures that can be modeled. With this in mind, the Bozzolo-Ferrante-Smith (BFS) method for alloys was designed to overcome these limitations, with the intent of providing an useful tool for the theoretical prediction of fundamental properties and structure of complex systems. After a brief description of the BFS method, its use for the determination of site substitution schemes for individual as well as collective alloying additions to intermetallic systems is described, including results for the concentration dependence of the lattice parameter. Focusing on B2 NiAl, FeAl and CoAl alloys, the energetics of Si, Ti, V, Cr, Fe, Co, Ni, Cu, Zr, Nb, Mo, Ru, Hf, Ta and W alloying additions are surveyed. The effect of single additions as well as the result of two simultaneous additions, discussing the interaction between additions and their influence on site preference schemes is considered. Finally, the BFS analysis is extended to ternary $L1_2$ (Heusler phase) alloys. A comparison between experimental and theoretical results for the limited number of cases for which experimental data is available is also included.

Introduction

During the past few years, a convergence of the computational sciences, condensed matter physics, chemistry and materials science has occurred in such a way as to provide valuable tools and expertise that could become of great utility in the design of novel, technologically useful materials. In the past, the development of new structural alloys and even small improvements to current alloys have mostly been performed through extensive experimental trial and error, which is both costly and time consuming. This approach is slowly changing, due to the concurrent effect of powerful computational techniques for different length scales, which provides basic knowledge needed at each step of new material development.

Of the several computer-based tools now available to the materials scientist, atomistic simulations based on sound theoretical methods have the potential to become useful at the early stages of materials design, due to their ability to provide fundamental information at the atomic level. Atomistic studies are broadly based on two types of approaches, first principles methods and semiempirical techniques. These techniques are useful in separate but complementary areas. First principles methods provide detailed electronic structure information, while semiempirical techniques are good for large scale simulations for the determination of bulk structural properties. Ideally, first-principles approaches are best suited for providing the most accurate and consistent framework for any study at the atomic level. However, the complexity of most real life problems convoluted with the overwhelming computational requirements for even simple systems have, to date, prevented first principles methods from becoming common and economical predictive tools beyond their current use. In fact, very few calculations exist that go beyond elementary binary alloys, and in some of these cases there are restrictions in scope and accuracy. This is gradually changing, and it is expected that future growth in computer power will correspondingly accelerate progress in this area. On the other hand, semiempirical methods based on quantum theory have enjoyed a great deal of attention in the last decade. This is mostly due to their computational simplicity, resulting in substantial progress in areas previously inaccessible to theoretical treatment, such as alloy structure analysis and design. However, most of the methods developed in the past have been severely restricted in the type and complexity of the systems amenable to such studies.

The purpose of these semiempirical methods is to provide an efficient but accurate way to compute the total energy of arbitrary atomic systems in terms of the geometrical configuration of the atoms, using approximations for the interactions between atoms. When applicable, the results contribute a great deal to the general understanding of the system under investigation. However, in most cases, the existing techniques are restricted to a limited number of systems or they require specific (and therefore non-transferable) parameterizations or potentials. Naturally, it would be desirable to overcome these limitations on the predictive power and applicability of these methods to increase their overall usefulness.

Recently, a new semiempirical method was developed with the goal of avoiding these limitations so that it could be adopted as a materials design tool. The Bozzolo-Ferrante-Smith (BFS) (1) method for alloys, based on quantum perturbation theory, is particularly designed to deal with complex systems and geometries. It has no constraints in its formulation that would limit the type or number of elements under consideration or on the number or type of resulting phases. The two distinguishing features of BFS are its novel way of modeling the alloy formation process - by breaking the process into two coupled transformations - and its extremely simple mathematical formulation, requiring the solution of a single transcendental equation for each transformation. These features of the BFS method are particularly useful when dealing with multicomponent systems, as will be shown in the present work dealing with the role of alloying additions to high temperature ordered intermetallics.

It is now well recognized that alloying additions to structural intermetallics are essential for the optimization of physical, chemical and mechanical properties. However, the role of these additions in controlling properties is poorly understood due to the lack of detailed microstructural information. As an example, in a NiAl+Ti system, Ti additions in the order of 2.5 to 3.0 at. % have been shown to result in a 200 to 5000 fold reduction in creep rate as compared to that of the binary NiAl (2). However, from a microscopic point of view, this behavior is not clearly understood, thus limiting our ability to modify and further improve the alloy (3).

In this work we take advantage of the versatility of the BFS method to tackle the problem of site substitutions of alloying additions to ordered intermetallics. Concentrating on transition metal rich B2 intermetallic alloys (NiAl, FeAl, CoAl), we studied the change in physical properties due to solid solution alloying additions, determined the substitutional site preference schemes, as well as interactions and changes due to multiple additives. To demonstrate the versatility of the BFS

method for this type of applications, we also analyzed the substitutional behavior of alloying additions in a selected group of $\text{Ni}_2(\text{Al},\text{X},\text{Y})$ Heusler alloys.

The BFS Method

Since its inception a few years ago, the BFS method has been applied to a variety of problems (1), ranging from bulk properties of solid solution fcc and bcc binary alloys to more specific applications like the energetics of bimetallic tip-sample interactions in an atomic force microscope and the effect of stoichiometry on the defect structure of NiAl (4) and FeAl alloys (5). The BFS method has also been used to deal with alloy surfaces (1). These previous studies provide a foundation for the work presented in this paper.

An interesting consequence of the simple mathematical formulation of the BFS method is that simple expressions can be derived for predicting the composition dependence of some bulk alloy properties based solely on pure component properties (the BF rule) (6). As it will be shown later in this work, these tools will become particularly useful when dealing with multiple additions to binary or higher order alloys (e.g. Ni_2AlTi).

In what follows, we provide a brief description of the operational equations of BFS in order to introduce some concepts used later on. The reader is encouraged to seek further details in previous papers (1,4-6) where a detailed presentation of the foundation of the method, its basis in perturbation theory and a discussion of the approximations made are clearly explained.

The BFS method provides a simple algorithm for the calculation of the energy of formation of an arbitrary alloy ΔH (the difference between the energy of the alloy and that of its individual constituents). In BFS, the energy of formation is written as the superposition of individual contributions of all the atoms in the alloy,

$$\Delta H = \sum_i (e'_i - e_i) = \sum_i \epsilon_i, \quad (1)$$

where e_i is the energy of an atom i in a pure elemental crystal and e'_i is the energy of the same atom in the alloy being studied. For each atom, we partition the contribution ϵ_i to the energy of formation ΔH into two parts: a strain energy and a chemical energy contribution. The first contri-

bution takes into account the atomic positions of the neighboring atoms to atom i , regardless of their chemical identity. For its calculation, we use the actual geometrical distribution of the atoms surrounding atom i , computed as if all of its neighbors were of the same species as atom i . In this sense, the BFS strain energy differs from the commonly defined strain energy in that the actual chemical environment is replaced by that of a single-element crystal. Its calculation is then straightforward and even amenable to first-principles techniques. In our work, we use Equivalent Crystal Theory (ECT) (7) for its computation, due to its proven ability to provide accurate and computationally economical answers to most general situations.

The chemical environment of atom i is evaluated in the computation of the BFS chemical energy term, where the surrounding atoms are forced to occupy equilibrium lattice sites corresponding to the reference atom i . Building on the concepts of ECT, BFS implements a straightforward approach for the calculation of the chemical energy, properly parameterizing the interaction between dissimilar atoms.

Thus defined, the BFS strain and chemical energy contributions take into account different factors, i.e. geometry and composition, computing them as isolated effects. A coupling function g restores the relationship between the two terms. The coupling function is defined in such away as to properly consider the asymptotic energy behavior where chemical effects are negligible for large separations between dissimilar atoms. Consequently, the contribution ϵ_i to the energy of formation ΔH from an individual atom i is then given by

$$\epsilon_i = \epsilon^S + g\epsilon^C \quad (2)$$

In what follows, we provide a brief description of the essential steps in the calculation of ϵ_i , which should be complemented with additional details described at length in Ref. 1. The strain energy contribution is obtained by solving the ECT perturbation equation (7)

$$NR_1^p e^{-\alpha R_1} + MR_2^p e^{-\left(\alpha + \frac{1}{\lambda}\right)R_2} = \sum_j r_j^p e^{-(\alpha + S(r))r_j} \quad (3)$$

where N and M are the number of nearest- and next-nearest neighbors respectively, and where p , l , α and λ are ECT parameters that describe element i (see Ref. 7 for definitions and details), r denotes the actual distance between the reference atom and each of its neighbors and $S(r)$ describes a screening function (7). The ECT parameters, together with the LMTO results, uniquely describe the physical properties of the element: p is related to the principal quantum number n ($p = 2n-2$), α parameterizes the electron density in the overlap region between two atoms, l is a screening parameter that takes into account atoms located at distances greater than nearest-neighbor distances, and λ is a scaling parameter that ensures that the dependence of the binding energy per atom as a function of lattice parameter follows satisfies the universal binding energy relationship of Rose et al. (8). The sum runs over nearest and next nearest neighbors. Eq. 3 is solved for a_S , the lattice parameter of the strain equivalent crystal, where the reference atom i has the same energy as it has in the geometrical environment of the alloy. R_1 and R_2 denote the nearest- and next-nearest neighbor distances in this equivalent crystal and are therefore related to the unknown a_S . Once the lattice parameter of the strain equivalent crystal a_S is determined, the BFS strain energy contribution is computed using the universal binding energy relation of Rose et al. (8), which contains all the relevant information concerning a single-component system:

$$\epsilon^S = E_C \left(1 - (1 + a_S^*) e^{-a_S^*} \right) \quad (4)$$

where E_C is the cohesive energy of atom i and where the scaled lattice parameter a_S^* is given by

$$a_S^* = q \frac{(a_S - a_e)}{l} \quad (5)$$

where q is the ratio between the equilibrium Wigner-Seitz radius and the equilibrium lattice parameter a_e . The values of the equilibrium lattice parameter a_e , the cohesive energy E_C and the bulk modulus B_0 for the bcc phase of all the elements used in this work are displayed in Table 1. These parameters are obtained from first principles, all-electron, density functional calculations of the elemental constituents in the symmetry of the alloy (i.e., bcc-Ni, bcc-Al, etc.). The particular

LMTO results				ECT parameters			
Atom	Lattice Parameter (Å)	Cohesive Energy (eV)	Bulk Modulus (GPa)	p	α (Å ⁻¹)	λ (Å ⁻¹)	l (Å)
Ni	2.752	5.869	249.2	6	3.067	0.763	0.2716
Al	3.192	3.942	77.3	4	1.8756	1.038	0.3695
Cr	2.837	4.981	286.1	6	2.8580	0.646	0.2300
Ti	3.213	6.27	121.0	6	2.8211	1.0476	0.3728
Cu	2.8225	4.438	184.55	6	3.0492	0.7615	0.2710
Co	2.7347	6.406	285.81	6	3.4779	0.7469	0.2658
Zr	3.5525	7.353	93.77	8	3.4641	1.2257	0.4362
Hf	3.4942	7.411	113.02	10	4.3132	1.1302	0.4022
Ta	3.3091	9.310	205.06	10	4.4230	0.9664	0.3439
Nb	3.3165	7.844	179.41	8	3.5099	0.9472	0.3371
Si	3.0701	4.654	99.99	4	1.9773	1.0158	0.3615
Fe	2.7423	6.071	311.53	6	3.0939	0.6955	0.2475
Mo	3.1781	7.195	273.54	8	3.5050	0.7506	0.2671
V	2.9770	7.512	199.01	6	3.0050	0.9290	0.3306
W	3.1932	9.953	315.98	10	4.4395	0.8194	0.2916
Ru	3.0700	7.664	338.32	8	3.6116	0.7086	0.2522

Table 1. Linear-muffin tin orbital (LMTO) results for the lattice parameter, cohesive energy and bulk modulus for the bcc phases of all elements listed. The last four columns display the resulting Equivalent Crystal Theory (ECT) (7) parameters determined from the LMTO results. p is related to the principal quantum number n for the atomic species considered ($p=2n-2$), a parameterizes the electron density in the overlap region between two neighboring atoms, λ is a screening factor for atoms at distances greater than nearest-neighbor distance and l is a scaling length needed to fit the lattice parameter dependence of the energy of formation with the universal binding energy relationship of Rose et al. (8).

implementation used is the Linear-Muffin-Tin Orbitals (LMTO) method (9) in the Atomic Sphere Approximation. The ensuing ECT parameters p , l , λ , and a_e are also included in Table 1.

The BFS chemical energy is obtained by a similar procedure. As opposed to the strain energy term, the surrounding atoms retain their chemical identity, but are forced to be in equilibrium lattice sites of an equilibrium (otherwise pure) crystal i . The BFS equation for the chemical energy is given by

$$NR_1^{p_i} e^{-\alpha_i R_1} + MR_2^{p_i} e^{-\left(\alpha_i + \frac{1}{\lambda_i}\right) R_2} = \sum_k \left(N_{ik} r_{1k}^{p_i} e^{-\alpha_{ik} r_{1k}} + M_{ik} r_{2k}^{p_i} e^{-\left(\alpha_{ik} + \frac{1}{\lambda_i}\right) r_{2k}} \right) \quad (6)$$

where N_{ik} and M_{ik} are the number of nearest- and next-nearest neighbors of species k of atom i .

The chemical environment surrounding atom i is reflected in the parameters α_{ik} , given by

$$\alpha_{ik} = \alpha_i + \Delta_{ki} \quad (7)$$

	Ni	Al	Cr	Ti	Cu	Co	Zr	Hf
Ni		-.06078	-.03588	-.09062	.01914	-.05384	-.12210	-.12681
Al	.09160		-.01524	-.08649	.05438	.17971	-.06367	.25061
Cr	.22482	-.01696		-.06107	.02449	.09571	-.11502	-.08881
Ti	.49580	.23399	.07343		.20565	.67092	-.05062	.36712
Cu	-.01708	-.04993	-.01180	-.07356		.13897	-.06767	.13561
Co	.14364	-.06792	-.02624	-.09593	-.05734		-.06399	-.13074
Zr	1.00755	-.04861	.40891	-.01583	-.04778	-.05068		.14942
Hf	.45749	-.07141	.01656	-.09376	-.07043	.54726	-.07487	

Table 2 BFS interaction parameters Δ_{XY} (first subindex indicates the row, the second indicates the column) and Δ_{YX} (in \AA^{-1}) for X-Y alloys (X, Y = Ni, Al, Cr, Ti, Cu, Co, Zr, Hf), determined by fitting the lattice parameter and energy of formation of the corresponding B2 compounds via LMTO.

where the BFS parameters Δ_{ki} (a perturbation on the single-element ECT parameter α_i used in Eq. 3) describe the changes of the wave function in the overlap region between atoms i and k . Once Eq. 6 is solved for the equivalent chemical lattice parameter a_C , the BFS chemical energy is computed using

$$\varepsilon^C = \gamma_i E_C^i \left(1 - (1 + a_C^*) e^{-a_C^*} \right) \quad (8)$$

where $\gamma_i = 1$ if $a_C^* > 0$ and $\gamma_i = -1$ if $a_C^* < 0$. The scaled chemical lattice parameter is given by

$$a_C^* = q \frac{(a_C - a_e)}{l_i} . \quad (9)$$

Finally, as mentioned above, the BFS chemical and strain contributions are linked by a coupling function g which describes the influence of the geometrical distribution of the surrounding atoms on the relevance of the chemical effects, and is given by

$$g_i = e^{-a_s^*} \quad (10)$$

where the scaled lattice parameter a_s^* is defined in Eq. (5).

In this work we use the BFS interaction parameters, Δ_{ki} , determined following the procedure outlined in Ref. 4. In order to provide parameters to the BFS method, we need to calculate the equilibrium properties of the elemental solid for the same symmetry as the compound to be studied, since BFS is referenced to the ground state properties of the system in that symmetry. Once these parameters are computed, they remain the same for any other calculation involving any of these elements as related to the given crystal symmetry, requiring no further adjustment or replacement. A partial list of the most relevant parameters is included in Table 2.

Results and Discussion

a. Single alloying additions to binary B2 compounds

While many aluminide-based intermetallic compounds have high melting temperatures, excellent oxidation resistance and low density, they are limited in actual structural applications due to the lack of sufficient room temperature ductility and elevated-temperature creep strength. Ternary and higher order elemental additions can alter these basic properties and, therefore, a general understanding of the substitutional site preference schemes could be of great help in the alloy design process. In this section, we perform BFS analyses of the site substitution patterns of ternary and higher order additions to NiAl, FeAl and CoAl.

The results quoted in this paper are based on BFS calculations of the energetics of a 72-atom cell in the AB B2 structure. This number of atoms is sufficient to study site substitutions of relevance to this work. A and B represent the two simple cubic sublattices of the B2 compound and X represents a ternary alloying addition. From the basic 72-atom computational cell we build a catalogue of several atomic configurations, each describing a specific site substitutional scheme. We introduce a convenient notation for such configurations: X(A) denotes an atom X substituting for

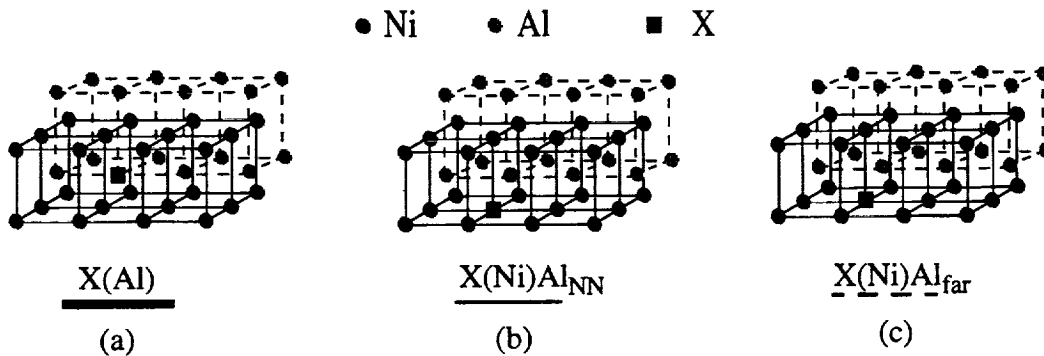


Figure 1: (a) An X atom occupying an Al site, (b) a Ni site with the Ni atom occupying the available Al site, at nearest-neighbor distance from each other, and (c) same as (b), but with the substitutional and antistructure atoms separated by a distance greater than the equilibrium nearest-neighbor distance. Ni and Al atoms are denoted by black and grey circles, respectively. The alloying addition is denoted with a solid square.

an atom A on the A sublattice, and X(A)B denotes the same case but with the displaced A atom occupying a site in the B sublattice. In this second case, we distinguish between the pair of defects X-A being nearest neighbors of each other (labeled NN in the figures) and the pair being separated by distances greater than that (labeled 'far' in the figures). Fig. 1 shows the simplest case, when just one atom (representing the alloying addition) occupies either an Al site (X(Al), Fig. 1.a) or a Ni (or Fe, Co in FeAl or CoAl alloys) site (X(Ni)Al), with the Ni atom forming an antistructure defect by occupying an Al site in a $\text{Ni}_{50}\text{Al}_{48.61}\text{X}_{1.39}$ alloy. Figs. 1.b and 1.c distinguish between the different relative locations of the substitutional atom and the antistructure atom. For simplicity and also because most alloying additions are made at the expense of Al, we will hold the transition metal composition constant at 50 at. % in most of the calculations unless otherwise noted. We could just as easily do the same calculations for substoichiometric transition metal compositions by taking into account vacancies in the calculations but space and actual interest in transition metal poor compositions preclude a discussion of those alloys in the present paper.

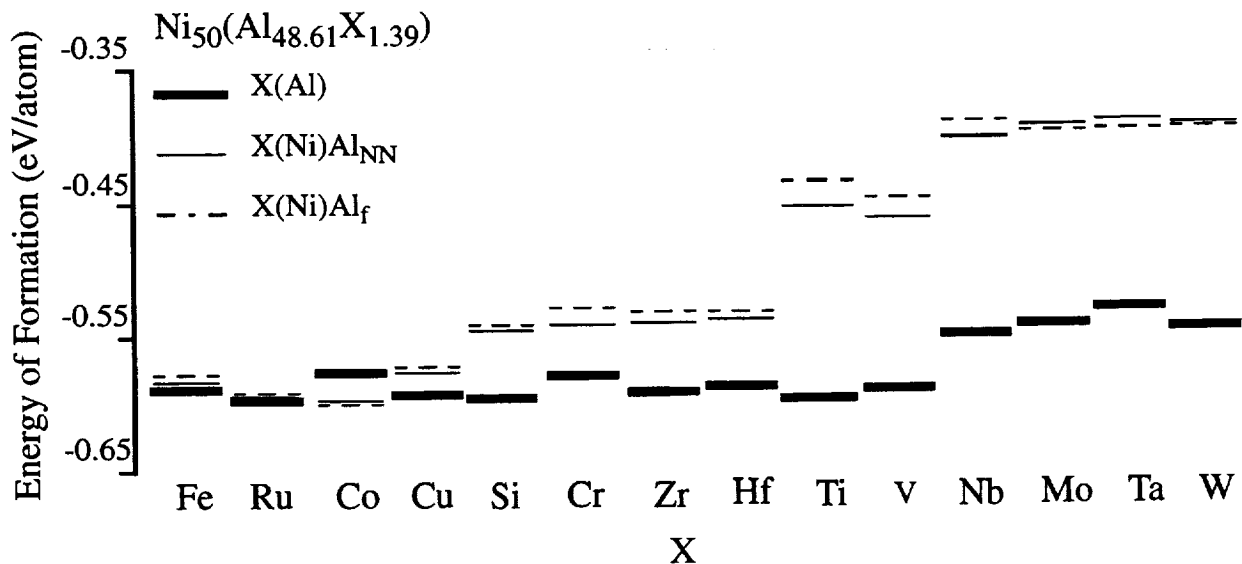


Figure 2: Energy spectrum for alloying additions to $\text{Ni}_{50}(\text{Al,X})_{50}$. The thick solid line corresponds to X(Al) defects (see Fig. 1.a), whereas thin solid lines and dashed lines correspond to X(Ni)Al defects as shown in Figs. 1.b and 1.c, respectively.

The site preference of the alloying addition is determined by computing the energy of formation of each cell and comparing the values obtained. However, determining the configuration with the lowest defect energy might not be sufficient for understanding the precise behavior of the additive. While it is true that the configuration with the lowest energy is the most likely to be found, it is important to consider the difference in energy between configurations describing different types of substitution patterns. If the difference between X(Al) and X(Ni)Al is significant, it is to be expected that atoms X will always occupy Al sites. Experimental difficulties in determining the site preference of certain elements could be related, among other factors, to the size of this energy gap. Moreover, we will see later that the interplay between several simultaneous additions can drastically change the behavior observed when each addition is considered individually, making the analysis of higher energy configurations even more important.

NiAl: In order to highlight the energy differences between various atomic arrangements, we present the results in the form of an 'energy spectrum'. Fig. 2 shows a spectrum of the energies of formation of the configurations described in Fig. 1 (for one atom of the alloying addition in the 72-atom cell), for several different elemental additions to NiAl. A wide range of behaviors is immediately apparent. In order to categorize the difference, we grouped the various elements considered by the magnitude of the energy gap, G (defined as the difference in energy between the lowest energy level and its immediately higher energy level, relative to the energy of the lowest-lying state). In doing so, we find four distinct groups: (a) Fe and Ru, with a gap of less than 1%, a negligible energy difference that is well within the fluctuations in the parameters used for this calculation, (b) Co and Cu, showing a small but distinguishable gap, (c) Si, Cr, Zr, Hf with a well defined gap and (d) Ti, V, Nb, Mo, Ta and W with a gap that is over 20% of the energy of formation of the defect. These last two groups are also characterized by the fact that all the additives considered mostly occupy Al sites.

In order to consider the possibility of changes in site preference with changes in concentration, we performed similar calculations, also in a 72-atom cell, for a number of configurations, corresponding to a $\text{Ni}_{50}\text{Al}_{47.22}\text{X}_{2.38}$ alloy. It should be noted that even if this concentration is greater than the solubility limit for X in NiAl alloys, it is feasible to compute the energetics of X in solid solution in NiAl, in spite of the fact that a second phase might form at that concentration. The calculation is based on a predefined atomic distribution, which may or may not reflect the correct ground state structure for that composition. This issue has been addressed in our previous

work on the effect of Ti and Cr additions to NiAl (10). In this work, we disregard the possibility of precipitate formation for the sake of investigating general trends for this set of candidate alloying additions.

Fig. 3 displays some of the possible configurations included in the catalogue of possible structures composed of two solute atoms in a 72-atom cell, showing only those sections of the cell affected by the presence of the alloying additions and the different resulting defect structures. Fig. 4 shows the energy spectrum corresponding to this set of configurations. Because of the larger

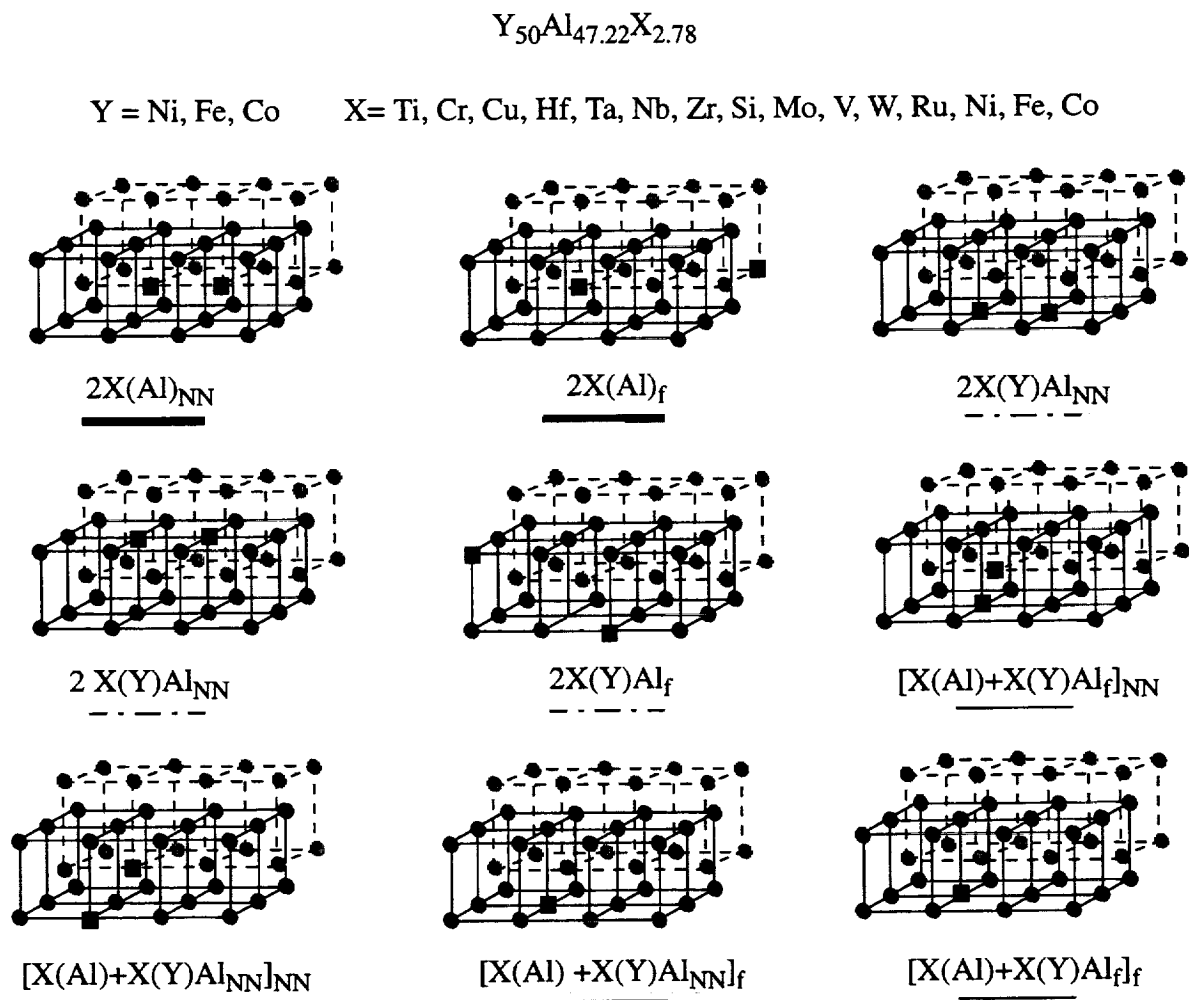


Figure 3: Configurations for two atoms in a 72-atom cell. A section of the cell containing the defect is shown. Y atoms (Ni, Fe, Co in NiAl, FeAl and CoAl, respectively) are indicated with solid black disks, Al atoms with grey disks and the additive X with a solid square.

number of possible defects due to their relative location in the lattice, the spectrum now includes 'bands' of states corresponding to the three main types of defects: the two solute atoms occupying Al sites (thick lines), the two solute atoms occupying Ni sites with the displaced Ni atoms in Al sites (dashed lines), and a combination of both type of defects (thin solid lines). This energy spectrum can be seen as an extension of the one shown in Fig. 2. A comparison with the single atom additions (lower concentration) provides information on the changes in the energy gaps due to the

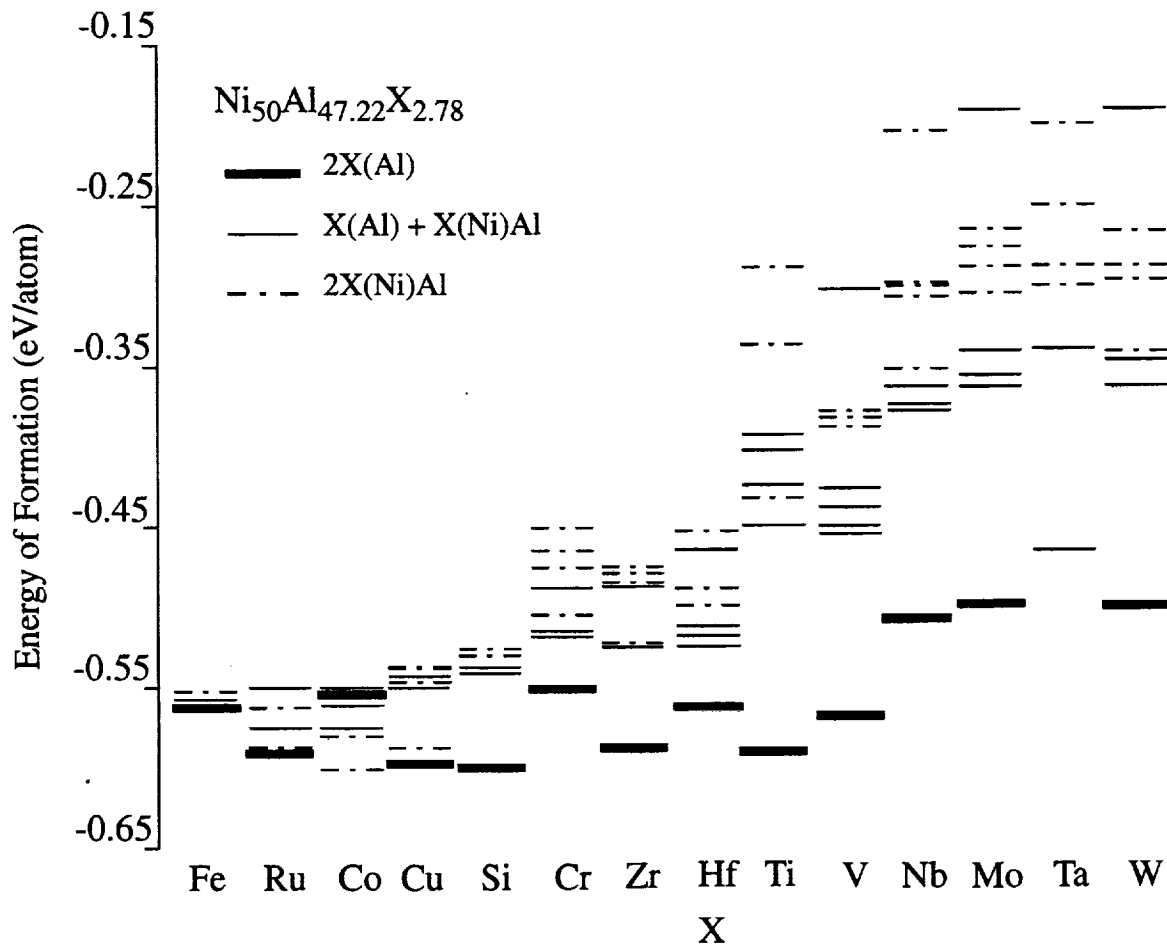


Figure 4: Energy spectrum of the configurations shown in Fig. 3. For each element, the different energy states are grouped depending on the type of defect: two X atoms in Al sites (solid thick line), one X atom in an Al site and one in a Ni site (thin solid line) and both X atoms in Ni sites (dashed lines). In those cases where the X atom occupies a Ni site, an antistructure defect is also created. The different levels for the same type of defect correspond to the differences due to the relative location of the defects with respect to each other.

Ni ₅₀ (Al+X) ₅₀			
Ni sublattice	No strong preference	Al sublattice	Experiment/Theory
Co, V	Ti, Cr, Fe, Cu	Zr, Nb, Mo, Hf, Ta, W	Theoretical model (11) Allaverdoba et al.
Fe, Co, Cu		Ti, V, Cr, Zr, Nb, Hf, Ta, W	Constitution diagrams (12)
	0.1 eV difference between Fe(Al), Fe(Ni)Al	Fe	First-principles calculations (13) Fu and Zou
Co (for $x_{Al} > 42.8 \text{at}\%$)		Cr, Fe, V. Co (for $x_{Al} < 42.8 \text{at}\%$)	Theoretical Model (14) Kao et al.
	Ti, V, Cr, Zr, Nb, Hf, Ta, W (both sites when unfilled with constituents)	Si	Pseudo ground state model (15) Hosoda et al.
		Fe	ALCHEMI (16) Anderson et al. , X-ray (EXAFS)(17)Chartier et al, Atom probe field ion microscopy (18) Duncan et al.
Fe, Co, Cu		Ti, V, Cr, Zr, Nb, Mo, Hf, Ta, W	X-ray diffraction analysis (11) Allaverdoba et al.
		Cr	ALCHEMI (19)Field et al. , ALCHEMI (20)Cotton et al.
		Ti	ALCHEMI (2) Kitabjian et al.
		V	ALCHEMI (21), Munrow et al.
Co	Fe, Ru, Cu (0.01 eV difference between X(Al)/ X(Ni)Al)	Fe, Ru, Cu, Si, Cr, Zr, Hf, Ti, V, Nb, Mo, Ta, W	BFS method (this work)

Table 3 Comparison between experimental (light shaded cells) and theoretical results for site preference of alloying additions in Ni(Al+X) alloys.

higher concentration of the alloying additions, and its effect on the site preference scheme. For example, a larger number of Ti atoms leaves the energy of the Ti(Al) level almost unchanged, while the Ti(Ni)Al levels (dashed lines in Fig. 2, dashed/dotted lines in Fig. 4) are clearly pushed toward higher energies, increasing the preference of Ti for Al sites. Fig. 4 also shows that, for the atomic species considered and the range of concentrations studied, there is no change in the basic site preference scheme with concentration.

A comparison of the BFS results with experiment and other types of theoretical calculations is provided in Table 3. In general, the BFS results are in excellent agreement with experiment and are consistent with other theoretical calculations. Unfortunately, few experimental results exist and most theoretical calculations have been performed for a rather small number of elements, limiting the comparison to the few cases available. Still, the available data is sufficient to put the BFS technique into proper perspective.

There is agreement between all the theoretical models and the experimental results with BFS predictions for the site preference of Co, with the exception of the pseudo ground state model of Hosoda et al. (15), where a critical composition ($x_{Al} = 42.8$ at. % Al) is determined for a change in site preference behavior. Above this critical concentration, Co is expected to occupy Ni sites. The site preference of Fe in NiAl has been the subject of several detailed studies due to the difficulty in establishing its behavior. In our work, Fe is found to have a very small value of G , with a slight preference for Al sites at zero temperature. This is in agreement with the detailed first principles study of Fu and Zou (13), who found a small value (0.1 eV) for the energy difference between the two types of defect. Several experimental studies (16-18) confirm the preference of Fe for Al sites. The BFS results for all the other alloying additions (Si, Cr, Zr, Hf, Ti, V, Nb, Mo, Ta and W) are in agreement with all the available experimental studies : Cr (11,19-20), Ti (2, 11), V (11, 21) and Zr, Nb, Mo, Hf, Ta, W (11).

For completeness, we summarize the numerical results for all the Ni(Al,X) alloy configurations in Table 4. For each entry, we list the energy of formation (in eV/atom) and the equilibrium lattice parameter of the resulting alloy. This value of the equilibrium lattice parameter is obtained by minimizing the energy of formation of every configuration with respect to isotropic expansions or compressions of the periodic cell. The changes in lattice parameter with elemental additions to Ni(Al,X) are shown in Fig. 5. The results obtained can be used to parameterize linear expressions for the dependence of the lattice parameter with concentration $a(x)$. In order to free these expres-

Table 4 Energies of formation (in eV/atom) and lattice parameter (in Å) for the defect configurations shown in Figs. 1 and 3 for NiAl+X alloys. The shaded boxes denote the lowest energy state. The elements are grouped according to the value of the energy gap G (see text).

Ni(Al + X)	Fe	Ru	Co	Cu	Si	Cr	Zr	Hf	Ti	V	Nb	Mo	Ta	W
X(Al)	-5.810 2.8460	-5.856 2.8546	-5.7801 2.8471	-5.9428 2.8468	-6.0566 2.8488	-5.8084 2.8483	-5.8886 2.8611	-5.8421 2.8633	-5.9550 2.8380	-5.8552 2.8311	-5.5237 2.8658	-5.4532 2.8664	-5.3264 2.8690	-5.4840 2.8656
X(Ni)Al _{NN}	-5.8044 2.8476	-5.9211 2.8545	-5.7845 2.8475	-5.7714 2.8484	-5.7103 2.8517	-5.5301 2.8525	-5.4042 2.8624	-5.3946 2.8632	-4.5433 2.8664	-4.6273 2.8623	-4.0677 2.8771	-3.9119 2.8783	-3.9107 2.8801	-3.9176 2.8800
X(Ni)Al _f	-5.7777 2.8480	-5.8943 2.8547	-5.7555 2.8485	-5.7555 2.8485	-5.6541 2.8522	-5.2772 2.8532	-5.3695 2.8625	-5.2923 2.8639	-4.3065 2.8687	-4.4306 2.8642	-3.9795 2.8778	-4.0046 2.8760	-3.9801 2.8791	-3.9195 2.8792
2X(Al) _{NN}	-5.6611 2.8433	-5.8586 2.8593	-5.5159 2.8444	-5.6859 2.8439	-6.0476 2.8476	-5.8577 2.8467	-5.9141 2.8726	-6.0000 2.8723	-6.8510 2.8582	-6.8522 2.8522	-6.8160 2.8750	-6.8776 2.8776	-6.8813 2.8813	-6.8159 2.8798
2X(Al) _f	-5.6711 2.8472	-5.8835 2.8590	-5.5303 2.8443	-5.6554 2.8437	-6.0476 2.8476	-5.8577 2.8466	-5.9141 2.8721	-6.0000 2.8722	-6.8510 2.8580	-6.8522 2.8522	-6.8160 2.8752	-6.8776 2.8778	-6.8814 2.8814	-6.8159 2.8801
2X(Ni)Al _{NN}	-5.5900 2.8449	-5.8183 2.8588	-5.9827 2.8393	-5.5200 2.8469	-5.4255 2.8531	-4.8003 2.8538	-4.8000 2.8752	-4.8154 2.8762	-3.8931 2.8748	-3.8287 2.8687	-3.0694 2.8946	-2.7383 2.8972	-2.6585 2.9015	-2.8185 2.8995
X(Ni)Al _{NN} +X(Ni)Al _f	-5.5516 2.8457	-5.7848 2.8590	-5.4940 2.8471	-5.4940 2.8471	-5.3325 2.8539	-4.5928 2.8557	-4.7614 2.8750	-4.6807 2.8770	-2.8490 2.8853	-3.0411 2.8765	-2.1011 2.9043	-1.9673 2.9030	-1.9600 2.9083	-1.9038 2.9075
[X(Ni)Al _{NN} +X(Al)] _{NN}	-5.6276 2.8435	-5.5827 2.8627	-5.7575 2.8417	-5.6856 2.8453	-5.6838 2.8509	-5.1709 2.8507	-4.9213 2.8762	-5.0076 2.8761	-4.3285 2.8717	-4.5483 2.8625	-3.7185 2.8884	-3.6288 2.8893	-3.4710 2.8933	-3.6205 2.8926
[X(Ni)Al _{NN} +X(Al)] _f	-5.6254 2.8437	-5.8491 2.8589	-5.7686 2.8417	-5.6835 2.8453	-5.7156 2.8505	-5.1265 2.8508	-5.2796 2.8734	-5.2263 2.8742	-4.4870 2.8703	-4.4589 2.8633	-3.6208 2.8891	-3.4006 2.8912	-3.2804 2.8951	-3.4496 2.8938
[X(Ni)Al _f +X(Al)] _f	-5.5994 2.8442	-5.8252 2.8591	-5.7716 2.8417	-5.6646 2.8455	-5.6582 2.8510	-5.0534 2.8515	-5.2489 2.8735	-5.1291 2.8749	-4.2500 2.8725	-4.2600 2.8652	-3.5248 2.8899	-3.4806 2.8891	-3.3389 2.8942	-3.4414 2.8931
[X(Ni)Al _f +X(Al)] _{NN}	-5.6120 2.8439	-5.5723 2.8628	-5.7766 2.8416	-5.6821 2.8453	-5.6355 2.8513	-5.1039 2.8513	-4.8979 2.8762	-4.9271 2.8767	-4.0953 2.8739	-4.3514 2.8644	-3.5690 2.8898	-3.5910 2.8888	-3.4439 2.8934	-3.5260 2.8930
[2X(Ni)Al] _f	-5.6249 2.8437	-5.8513 2.8589	-5.7681 2.8417	-5.6826 2.8453	-5.7152 2.8505	-5.1279 2.8508	-5.2823 2.8734	-5.2269 2.8742	-4.4777 2.8704	-4.4543 2.8633	-3.6030 2.8893	-3.3835 2.8914	-3.2654 2.8952	-3.4275 2.8940
[2X(Ni)Al] _{NN}	-5.5292 2.8462	-5.7746 2.8591	-5.4872 2.8471	-5.4872 2.8471	-5.2762 2.8545	-4.6236 2.8554	-4.7337 2.8750	-4.5893 2.8777	-3.4108 2.8793	-3.3878 2.8729	-2.9960 2.8947	-3.0338 2.8908	-2.9270 2.8980	-2.9639 2.8960

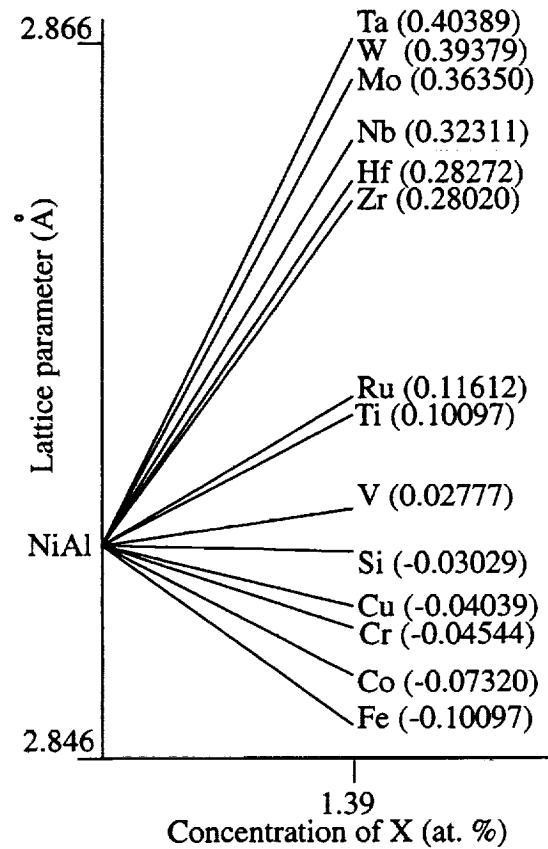


Figure 5: Lattice parameter as a function of concentration of several alloying additions X (X = Si, Ti, V, Cr, Fe, Co, Cu, Zr, Nb, Mo, Ru, Hf, Ta,W) to NiAl. The values of μ (Eq. 11) are given in parenthesis.

sions from their dependence on the end values (i.e. equilibrium lattice parameter of binary NiAl, a_{NiAl} determined by first principles methods (4)), we normalize $a(x)$ by a_{NiAl} , obtaining the general expression

$$\frac{a(x)}{a_{NiAl}} = 1 + \mu x. \quad (11)$$

where x is the concentration of the alloying addition. The values of μ are included in Fig. 5.

As mentioned before, the BFS method also allows for the derivation of simple expressions that provide an approximate value of μ based *only* on the single-element properties (lattice

parameter, bulk modulus and cohesive energy, as listed in Table 1). The BF rule (6) for the lattice parameter of the alloy as a function of concentration of each element is

$$a(x) = \frac{\sum_i x_i B_i a_i^2}{\sum_i x_i B_i a_i} \quad (12)$$

where a_i and B_i are the equilibrium lattice parameter and the bulk modulus, respectively, of element i in the symmetry of the alloy. In the particular case studied in this work, $XAl_{50-x}Y_x$, with $X = Ni, Fe, Co$, Eq. (12) becomes

$$a(x) = \frac{\frac{1}{2}a_X^2 B_X + \left(\frac{1}{2} - x\right)a_{Al}^2 B_{Al} + xa_Y^2 B_Y}{\frac{1}{2}a_X B_X + \left(\frac{1}{2} - x\right)a_{Al} B_{Al} + xa_Y B_Y} \quad (13)$$

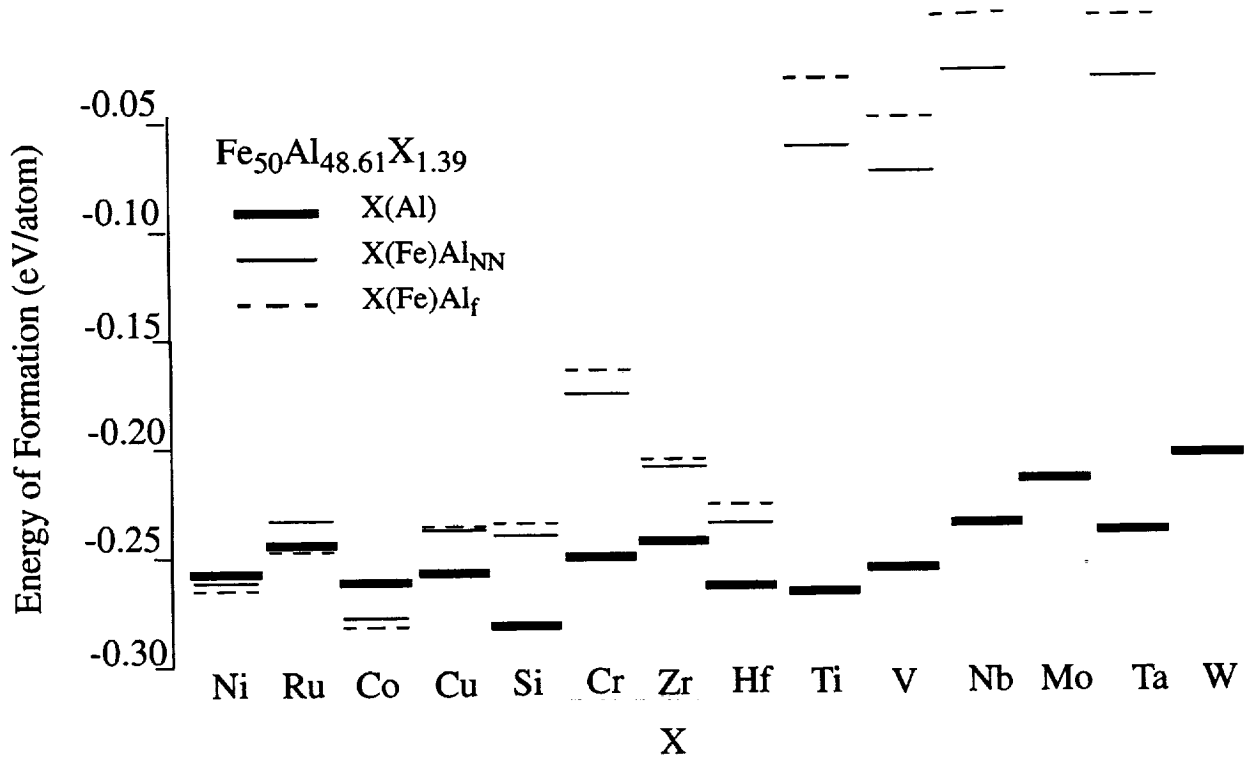


Figure 6: Energy spectrum for Fe (Al+X) alloys with alloying additions of X. See Fig. 2 for details concerning the type of defect structures modeled. .

from which the approximate value of μ can be derived. These expressions do not take into account specific ordered structures, therefore leaving out the strong bonding characteristics of these B2 compounds. However, in the case of several alloying additions, it is obviously a practical way of determining an approximation for the behavior of the lattice parameter with composition.

FeAl: Similar calculations were carried out for Fe(Al+X) alloys, following the same procedure used for NiAl. Fig. 6 displays the energy spectrum for a low concentration of the alloying addition X. The numerical results for all possible configurations, both for low and high concentration, are listed in Table 5 As for NiAl, the different alloying additions are ordered according to the relative magnitude of the energy gap between the two main site occupancy choices. Ni and Ru

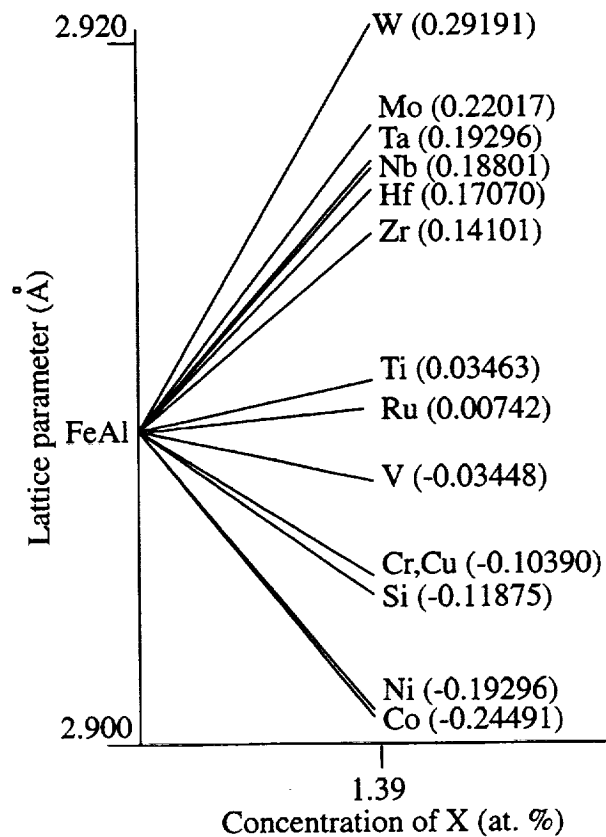


Figure 7: Lattice parameter as a function of concentration of several alloying additions X to

Table 5 Energies of formation (in eV/atom) and lattice parameter (in Å) for the defect configurations shown in Figs. 1 and 3 for NiAl+X alloys. The shaded cells represent the lowest energy configuration. The alloying additions are grouped according to the value of the energy gap G, listed below

FeAl + X	Ni	Ru	Co	Cu	Si	Cr	Zr	Hf	Ti	V	Nb	Mo	Ta	W
X(Al)	-2.5588 2.9022	-2.4491 2.9115	-2.6174 2.9009	-2.5685 2.9039	-2.8240 2.9083	-2.5045 2.9089	-2.4323 2.9148	-2.6421 2.9140	-2.6758 2.9095	-2.5489 2.9067	-2.3632 2.9157	-2.1585 2.9170	-2.3169 2.9150	-2.0227 2.9199
X(Fe)Al ₁₁ N	-2.6018 2.9088	-2.3334 2.9107	-2.7798 2.8987	-2.3729 2.9041	-2.4040 2.9063	-1.7679 2.9092	-2.0886 2.9160	-2.3458 2.9142	-0.6127 2.9259	-0.7731 2.9211	-0.2665 2.9338	.00061 2.9355	-0.2938 2.9346	.01648 2.9387
X(Fe)Al ₁₂ f	-2.6265 2.9002	-2.24810 2.9088	-2.8133 2.8989	-2.3570 2.9040	-2.3527 2.9066	-1.6647 2.9100	-2.0583 2.9160	-2.2716 2.9145	-0.2915 2.9288	-0.5054 2.9234	.00322 2.9365	.00337 2.9344	-0.00410 2.9368	.01753 2.9377
2X(Al) ₁₁ N	-2.4978 2.8963	-2.2803 2.9148	-2.6140 2.8939	-2.8998 2.8998	-2.8984 2.8984	-2.2588 2.8998	2.9136 2.9136	-2.6789 2.9118	-2.690 2.9107	-2.095 2.9130	1.84 2.9124	1.7860 2.9220	-2.196 2.9195	1.536 2.9313
2X(Al) ₁₂ f	-2.5132 2.8962	-2.2903 2.9147	-2.6329 2.8937	-2.8997 2.8997	-2.8984 2.8984	2.4016 2.8998	2.9116 2.9116	-2.6316 2.9116	-2.7425 2.9169	-2.4880 2.9124	-2.1250 2.9131	-1.7184 2.9220	-2.138 2.9195	-1.4548 2.9310
2X(Fe)Al ₁₁ N	-2.5656 2.8939	-2.0611 2.9135	-2.9075 2.8900	-2.1571 2.9002	-2.2450 2.9042	-1.1956 2.9080	-1.6278 2.9235	-2.0899 2.9206	.01639 2.9327	.01395 2.9257	.06343 2.9461	.12648 2.9503	.07041 2.9487	.14524 2.9553
X(Fe)Al ₁₁ N+X(Ni)Al ₁₂ f	-2.6261 2.8930	-2.2004 2.9109	-2.9985 2.8889	-2.1190 2.9000	-2.1454 2.9048	-0.8145 2.9111	-1.5424 2.9239	-2.0158 2.9204	.16719 2.9470	.13190 2.9367	.22949 2.9621	.25712 2.9611	.21900 2.9630	.28484 2.9674
[X(Fe)Al ₁₁ N+X(Al)] ₁₁ N	-2.5417 2.8951	-2.1798 2.9141	-2.7479 2.8921	-2.2409 2.9012	-2.5790 2.9020	-1.7655 2.9043	-1.8251 2.9226	-2.1334 2.9232	-0.6075 2.9279	-0.8725 2.9183	-0.1796 2.9402	.00432 2.9404	-0.2622 2.9405	.02857 2.9458
[X(Fe)Al ₁₁ N+X(Al)] ₁₂ f	-2.5573 2.8948	-2.1729 2.9139	-2.7987 2.8915	-2.3332 2.8999	-2.6192 2.9014	-1.6611 2.9050	-1.9166 2.9217	-2.3862 2.9210	-0.7012 2.9270	-0.7193 2.9195	-0.00731 2.9407	.03993 2.9433	-0.1041 2.9417	.06709 2.9491
[X(Fe)Al ₁₂ f+X(Al)] ₁₂ f	-2.5838 2.8943	-2.3191 2.9117	-2.8352 2.8910	-2.3151 2.8998	-2.5684 2.9017	-1.5541 2.9058	-1.8862 2.9217	-2.3129 2.9213	-0.3704 2.9299	-0.4431 2.9218	.02316 2.9434	.04357 2.9423	.01539 2.9439	.06909 2.9482
[X(Fe)Al ₁₂ f+X(Al)] ₁₁ N	-2.5872 2.8945	-2.2882 2.9124	-2.8075 2.8914	-2.2401 2.9010	-2.5422 2.9022	-1.6697 2.9049	-1.8112 2.9225	-2.0919 2.9232	-0.2930 2.9306	-0.6051 2.9206	.01384 2.9430	.01906 2.9408	.00182 2.9430	.04186 2.9463
[2X(Fe)Al ₁₂ f]	-2.5586 2.6626	-2.1754 2.9139	-2.7988 2.8915	-2.3344 2.8999	-2.6211 2.9014	-1.6629 2.9050	-1.9189 2.9216	-2.3843 2.9210	-0.6821 2.9272	-0.7098 2.9195	-0.0474 2.9410	.04236 2.9435	-0.00830 2.9419	.07029 2.9494
[2X(Fe)Al ₁₂ f] ₁₁ N	-2.6626 2.8978	-2.2429 2.9070	-3.0350 2.8888	-2.1554 2.8994	-2.1169 2.9048	-0.9489 2.9096	-1.5640 2.9235	-1.9454 2.9207	.08227 2.9382	.07285 2.9307	.11904 2.9508	.12086 2.9464	.11630 2.9525	.13187 2.9513

exhibit a negligible gap $G < 3 \%$ while Co and Cu show a clear distinction between the two possible levels ($3 < G < 10 \%$). All the other elements display a clear preference for Al sites, with Si, Cr, Zr and Hf having a distinct gap ($10 < G < 30 \%$) and the rest (Ti, V, Nb, Mo, Ta, W) showing preference for Al sites with excessively large gaps ($G > 70 \%$).

Completing the presentation of results for FeAl, Fig. 7 shows the change in lattice parameter with concentration for all the alloying additions considered in this work, also showing the corresponding slopes μ of the linear dependence of the lattice parameter on the ternary addition with concentration. Again, the slopes of the linear expressions for $a(x)$ were normalized to the LMTO-determined value for the lattice parameter of FeAl,

$$\frac{a(x)}{a_{FeAl}} = 1 + \mu x \quad (14)$$

where x is the concentration of the alloying addition. The values of μ are included in Fig. 7.

Unfortunately, very few theoretical or experimental results exist for Fe(Al+X) alloys. The preference of Ni and Co for Fe sites agree with the theoretical results of Allaverdova et al. (11). They also predict the same site preference for Cu and Cr, although they admit that their prediction for Cr is questionable. The small energy gap found for Cu in this work could be an explanation of the ambiguity found in their work. That is not the case for Cr, where BFS predicts a large gap favoring Al sites, as found experimentally by synchrotron X-ray diffraction experiments by Khosla (22), confirmed by the work of Munroe et al (21), who established the preference of Cr for Al sites by means of ALCHEMI and X-ray methods. First principles calculations using Local Density Functional theory by Fu and Zow (13) found Ti and Cr preference for Al sites and Ni preference with Fe sites, in complete agreement with our predictions. There is also excellent agreement with the quasichemical model introduced by Kao et al. (14), which predicts V preference for Al sites and Co and Ni preference for Fe sites. The authors point out that the predictions for other transition metal additions have large uncertainties and should not be used as basis of comparison.

One of the most comprehensive studies of site distribution of transition metals is the recent work of Anderson (23), which includes an ALCHEMI analysis of Ti, V, Cr, Mn, Co, Ni and Cu in FeAl. The BFS results for Co, Ni and Cu exhibit a very small energy gap G . The slight preference

of Co and Ni for Fe sites is in agreement with the ALCHEMI predictions, but Cu results are not. In these situations (i.e. small G), as noted before for Fe in NiAl, just the inclusion of entropic effects at finite temperature may or may not be sufficient to alter the preference scheme.

The most marked preference for Al sites is that of Ti, in agreement with our work, with 85 % of the alloying element occupying Al sites. The residual Fe site occupancy is explained by Anderson in terms of site equilibration kinetics, as diffusion of substitutional defects is required. Unfortunately, we have not included the possibility of vacancies in our calculation, as NiAl - the basis of our study- does not have structural vacancies for Ni-rich alloys. A more general catalogue, including vacancies, has been defined and tested in our previous work on binary FeAl (5). The defect structure (substitutions for Fe rich, triple defects for FeAl and Al-rich FeAl) was correctly determined, in agreement with experiment and other theoretical approaches.

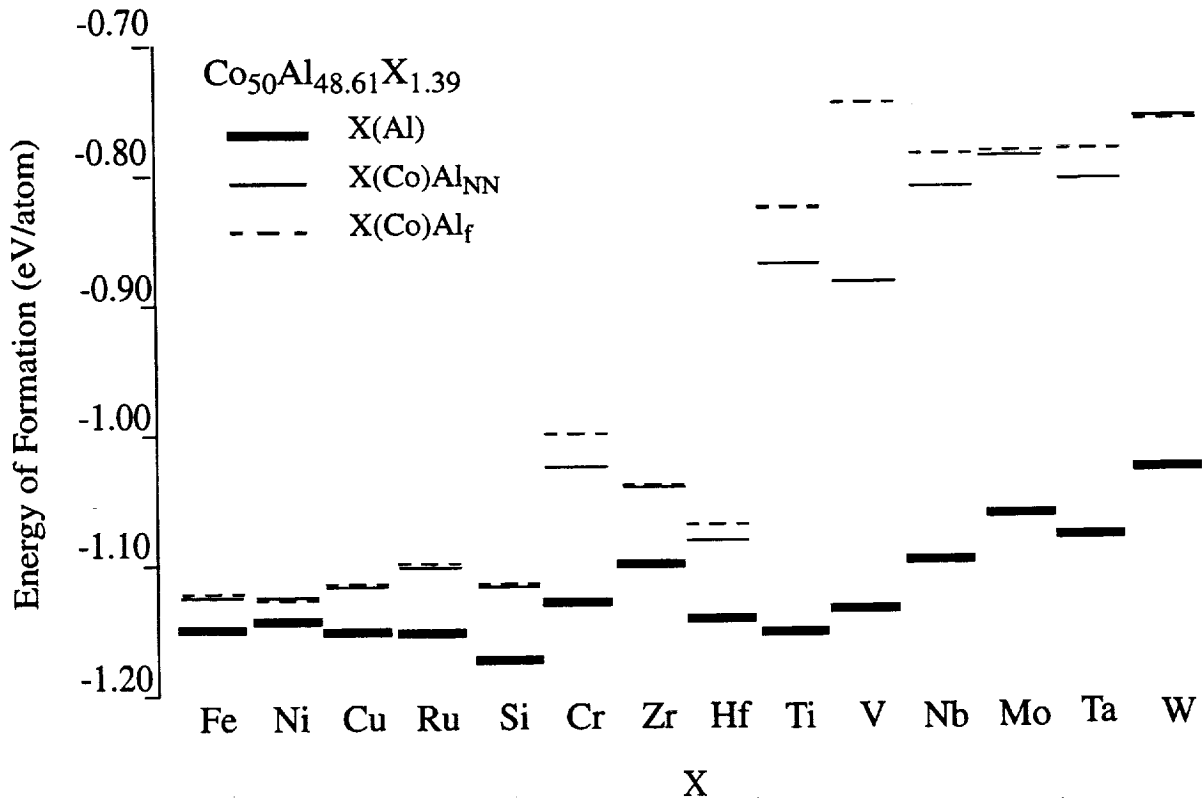


Figure 8: Energy spectrum for Co(Al+X) alloys with alloying additions of X. See Fig. 2 for details on the type of defect structures modeled.

Table 6 Energies of formation (in eV/atom) and lattice parameter (in Å) for the defect configurations shown in Figs. 1 and 3 for Co(Al+X) alloys. The shaded cells denote the lowest energy state. The elements are grouped according to the value of the energy gap G (see text).

CoAl + X	Fe	Ni	Cu	Ru	Si	Cr	Zr	Hf	Ti	V	Nb	Mo	Ta	W
X(Al)	-1.1277 2.7903	-1.1278 2.7896	-1.0990 2.7928	-1.1039 2.8004	-1.0980 2.7949	-1.0232 2.7994	-1.0469 2.8058	-1.0828 2.8038	-0.8740 2.8169	-0.8985 2.8121	-0.8218 2.8270	-0.7854 2.8309	-0.8172 2.8287	-0.7618 2.8349
X(Co)Al _{NN}	-1.1238 2.7908	-1.1280 2.7894	-1.0925 2.7932	-1.0951 2.8011	-1.0890 2.7956	-1.0072 2.8007	-1.0412 2.8062	-1.0712 2.8045	-0.8305 2.8205	-0.8622 2.8151	-0.7834 2.8302	-0.7846 2.8294	-0.7896 2.8310	-0.7636 2.8336
2X(Al) _{NN}														
2X(Al) _f														
2X(Co)Al _{NN}	-1.0883 2.7895	-1.0855 2.7885	-1.0384 2.7940	-1.0525 2.8085	-1.0364 2.7984	-0.9164 2.8048	-0.9378 2.8201	-1.0025 2.8166	-0.7376 2.8301	-0.7495 2.8234	-0.6601 2.8478	-0.5806 2.8560	-0.6338 2.8527	-0.5506 2.8624
X(Co)Al _{NN} +X(Ni)Al _f	-1.0838 2.7902	-1.0878 2.7881	-1.0232 2.7951	-1.0321 2.8100	-1.0192 2.7997	-0.8627 2.8091	-0.9234 2.8212	-0.9892 2.8172	-0.5463 2.8469	-0.5987 2.8364	-0.4563 2.8660	-0.4227 2.8680	-0.4593 2.8682	-0.3826 2.8757
[X(Co)Al _{NN} +X(Al)] _N	-1.1076 2.7871	-1.1052 2.7871	-1.0803 2.7910	-1.0552 2.8102	-1.0986 2.7933	-1.0086 2.7978	-0.9821 2.8163	-1.0277 2.8167	-0.8537 2.8216	-0.8947 2.8122	-0.7852 2.8378	-0.7401 2.8435	-0.7734 2.8409	-0.6986 2.8507
[X(Co)Al _{NN} +X(Al)] _f	-1.1077 2.7873	-1.1049 2.7871	-1.0803 2.7908	-1.0896 2.8059	-1.1017 2.7929	-0.9940 2.7988	-0.9880 2.8158	-1.0585 2.8144	-0.8667 2.8207	-0.8747 2.8137	-0.7677 2.8389	-0.6914 2.8474	-0.7451 2.8430	-0.6444 2.8552
[X(Co)Al _f +X(Al)] _f	-1.1034 2.7878	-1.1044 2.7870	-1.0733 2.7913	-1.0810 2.8065	-1.0918 2.7937	-0.9772 2.8001	-0.9814 2.8163	-1.0475 2.8151	-0.8227 2.8244	-0.8376 2.8167	-0.7282 2.8422	-0.6883 2.8462	-0.7160 2.8454	-0.6438 2.8541
[X(Co)Al _f +X(Al)] _{NN}	-1.1067 2.7874	-1.1085 2.7867	-1.0759 2.7913	-1.0493 2.8106	-1.0918 2.7938	-0.9938 2.7989	-0.9788 2.8165	-1.0199 2.8171	-0.8113 2.8252	-0.8587 2.8151	-0.7448 2.8412	-0.7237 2.8439	-0.7414 2.8435	-0.6845 2.8511
[2X(Co)Al] _f	-1.1074 2.7873	-1.1046 2.7871	-1.0804 2.7908	-1.0901 2.8058	-1.1015 2.7930	-0.9940 2.7988	-0.9879 2.8158	-1.0585 2.8144	-0.8640 2.8209	-0.8736 2.8138	-0.7642 2.8392	-0.6879 2.8477	-0.7420 2.8433	-0.6400 2.8556
[2X(Co)Al] _f NN	-1.0798 2.7907	-1.0895 2.7878	-1.0236 2.7950	-1.0328 2.8100	-1.0132 2.8001	-0.8773 2.8078	-0.9248 2.8210	-0.9777 2.8179	-0.6457 2.8378	-0.6683 2.8302	-0.5874 2.8539	-0.5886 2.8517	-0.5864 2.8564	-0.5688 2.8579

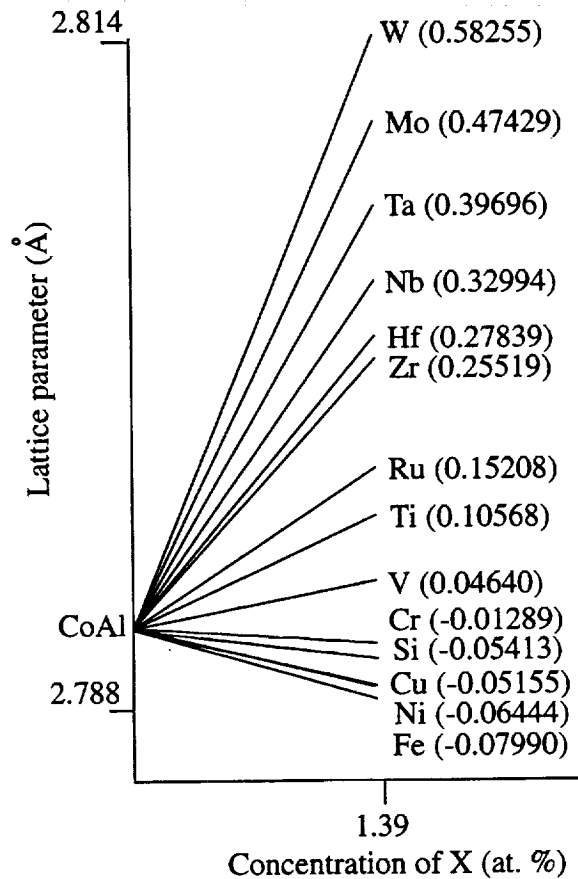


Figure 9: Lattice parameter as a function of concentration of several alloying additions X to CoAl. The values of μ (Eq. 14) are given in parenthesis.

CoAl: Having found agreement with available experimental and theoretical evidence for both NiAl and FeAl raises confidence in the BFS method and the parameterization used in this work. The parameters determined for the individual elements, as well as the BFS parameters Δ_{AB} calculated for all pairs A-B are unique and transferable, making it trivial to use them for the calculation of **any** other B2 alloy formed by the elements considered. It is therefore reasonable to extend the application of this methodology to CoAl, a system for which we could find no experimental data on the behavior of alloying additions in this compound in the current literature. Following the for-

mat of our previous examples, we display the BFS predictions for the site occupancy in Co(Al+X) alloys by showing the energy spectrum for single-atom substitutions in Fig. 8, and the complete set of results for the energy of formation and equilibrium lattice parameter as a function of composition in Table 6. The elements are grouped by the value of their energy gap G : Fe, Ni ($G < 2\%$); Cu, and Ru ($2 < G < 5\%$); Si, Cr, Zr and Hf ($5 < G < 10\%$) and Ti, V, Nb, Mo, Ta and W ($G > 20\%$) In addition, the change in lattice parameter is displayed in Fig. 9 (see Eq. 11).

To conclude the analysis of ternary additions to XAl ($X = \text{Ni, Fe, Co}$), we summarize the site preference scheme in Fig. 10, where we show, for each intermetallic compound, the site preference distribution. It should be noted that while helpful in obtaining a quick feel for the behavior of each element, there is no explicit consideration of the strong ordering tendencies that characterize these compounds. It is therefore to be expected that the BF rule predictions of the absolute values of the lattice parameter might not be as reliable as those obtained from full BFS calculations. As with the lattice parameter in Eq. 12, the bulk modulus, for arbitrary number or additions and con-

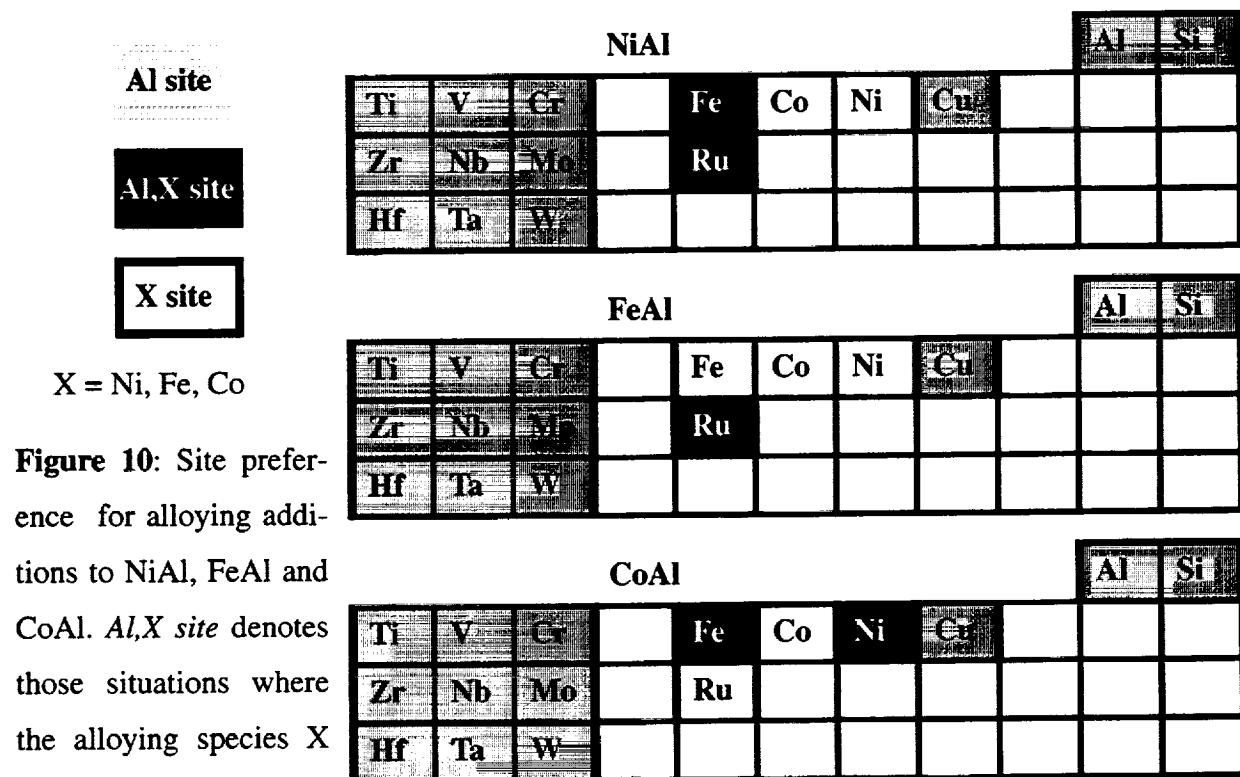


Figure 10: Site preference for alloying additions to NiAl, FeAl and CoAl. Al,X site denotes those situations where the alloying species X

centrations, can be computed for any of the alloys studied or for those that can be constructed from the elements parameterized in this work, by using the following expression

$$B(x) = \frac{\left(\sum_i x_i B_i a_i\right)^2}{\sum_i x_i B_i a_i^2} \quad (15)$$

where the single element values a_i are listed in Table 1. The values of B_i can be obtained from the definition of the scaling length l ,

$$l_i = \sqrt{\frac{E_C}{12\pi q B_i a_e}} \quad (16)$$

b. Double alloying additions to B2 compounds

Beyond examining all possible B2 alloys that can be composed of the 16 elements considered in this work (i.e. CuAl, etc.), the BFS method allows for a straightforward generalization to higher order additions, without any new determination of parameters and without any additional complexity in the calculations or the computer resources needed. A review of the description of the BFS method should convince the reader that no particular provision should be taken when increasing the number of elements in the system. The only additional effort consists of generating a larger ‘catalogue’ of possible atomic configurations than that used for the simple ternary case. We therefore constructed a sufficiently large catalogue of atomic distributions contemplating all the possible atomic arrangements and the ensuing defects for two or more simultaneous alloying additions to binary B2 intermetallic compounds. One of the many goals of such effort is to investigate the changes, if any, in site preference of individual atomic species in the presence of other alloying additions.

As can be seen in Fig. 1, some types of atoms might be susceptible to changing their substitutional behavior in the presence of other additions due to the small energy gap between different

configurations. Ti, for example, has a definite preference for Al sites in NiAl, a fact clearly proven experimentally and by any other theoretical calculation (2, 11, 12). The large energy gap between Ti(Al) and Ti(Ni)Al substitutions clearly support this fact. It is to be expected that the addition of a fourth element would be, in general, irrelevant in changing the behavior of Ti in NiAl. This can be seen in Fig. 11, which shows the energy spectrum of Ti in NiAl, and the changes it undergoes in the presence of a fourth element. A detailed analysis of this figure indicates that, in general, the Ti(Al) choice is not affected by any of the additions. The lower part of the spectrum is completely dominated by Ti(Al) defects (thick solid and dashed lines). Con-

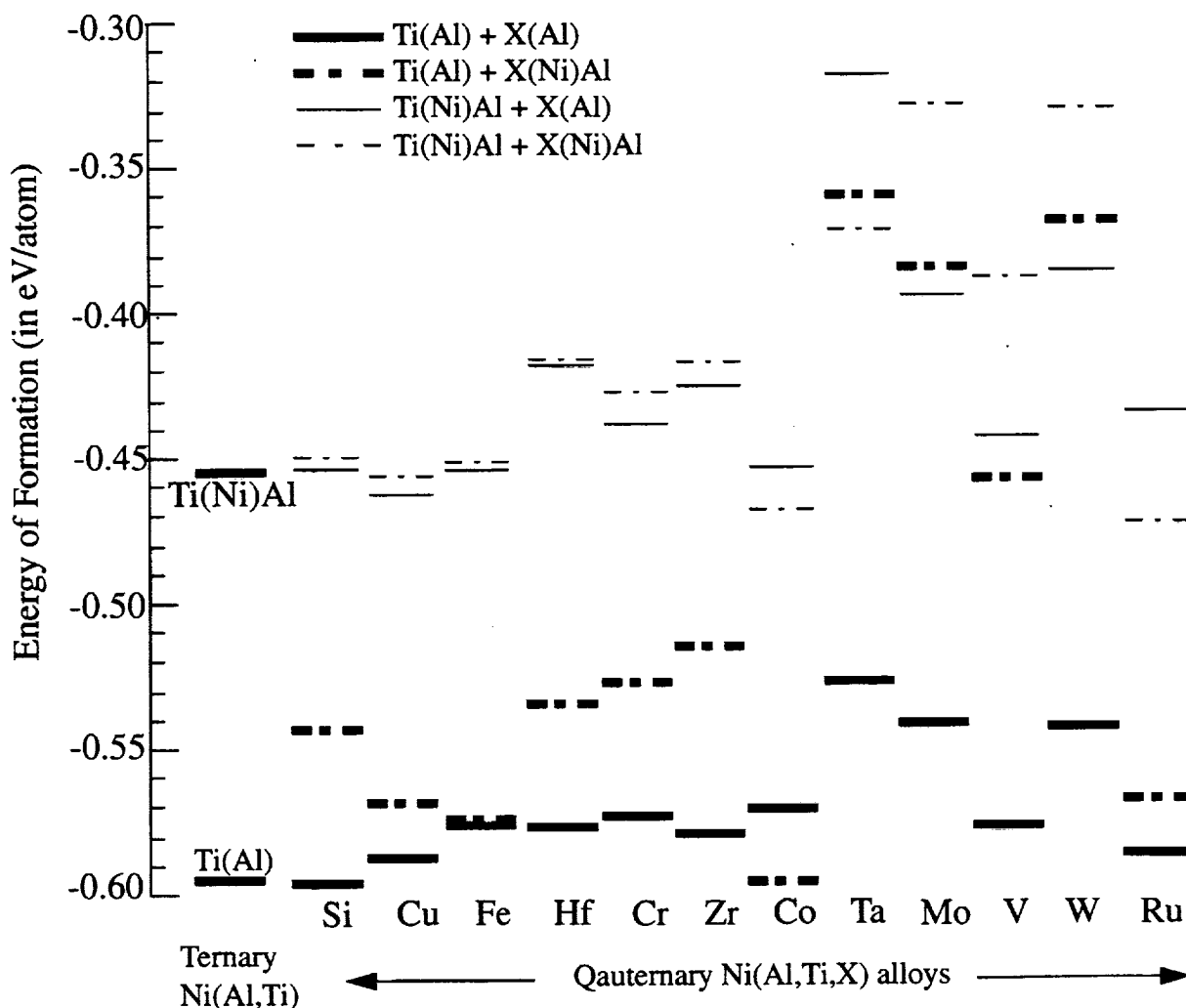


Figure 11: Energy spectrum of two simultaneous alloying additions to Ni(Al+X+Y) alloys. The first column shows the ternary case, Ni(Al,Ti) The subsequent columns describe the energetics of quaternary alloys with the defect structure indicated in the inset.

versely, the presence of Ti does not seem to affect the individual preference of the other elements. Fe, for example, has a minuscule energy gap when acting alone, and it continues to do so in the presence of Ti: Ti(Al) + Fe(Al) and Ti(Al)+Fe(Ni)Al defects are almost equivalent in energy.

The strong tendency of Ta, Mo, V and W for Al sites is emphasized in the presence of Ti, making Ti(Ni)Al substitutions slightly more favorable than Ti(Al), although they are all very high in energy to have any significance. The numerical results are displayed in Table 7, which in addition to the results plotted in Fig. 11 for Ni(Al+X) alloys, includes results for two-element additions to stoichiometric NiAl.

Co, on the other hand, benefits from the presence of Fe increasing its likelihood for choosing Ni sites with respect to its isolated behavior. The same effect is seen in Ru, but in favor of Al sites.

We could continue this analysis for all the possible combinations of alloying additions considered in this work, as well as extending it to include 3, 4 or more simultaneous additions, a calculation that would only entail the generation of the necessary catalogue of configurations. Such massive presentation of results is naturally beyond the limitations of this paper, and it will be published elsewhere. The main goal of this paper is to simply introduce the BFS method for this type of application with an appropriate illustration of typical results

c. Heusler structures

We conclude our analysis by considering single alloying additions to ternary Heusler phases. Once again, the complexity of the calculation depends on our ability to define the proper catalogue of configurations which will adequately describe the system at hand. We continue to use the same set of parameters that were used for the B2 compounds. While numerous Heusler phases exist, there is very little known about these alloys in terms of their physical properties, except for the lattice parameter of some alloys. No information on site preference of alloying additions seems to be available. Fig. 12 shows the most important site substitution schemes consistent with the structure of the Heusler phase (A atoms in one cubic sublattice, and B and C atoms in the other sublattice, in alternating corners of the cube). Table 8 lists the corresponding energies of formation and equilibrium lattice parameter for each one of these atomic arrangements, from which the site preference scheme can be extracted for a base Heusler compound of Ni₂AlTi.

NiAl+(Ti,X)	Hf	Zr	Ta	Cu	Co	Fe	Cr	Si
$Ni_{50}(Al,Ti,X)_{50}$								
Ti(Al)+X(Al)	-5340 2.8668	-5166 2.8679	-3619 2.8860	-5690 2.8524	-5709 2.8511	-5775 2.8500	-5293 2.8524	-5432 2.8575
Ti(Al)+X(Ni)Al	-5340 2.8668	-5166 2.8679	-3619 2.8860	-5690 2.8524	-5963 2.8484	-5767 2.8511	-5293 2.8563	-5432 2.8575
Ti(Ni)Al+X(Al)	-4140 2.8794	-4282 2.8782	-3709 2.8838	-4623 2.8616	-4543 2.8610	-4554 2.8608	-4403 2.8643	-4542 2.8653
Ti(Ni)Al +X(Ni)Al	-4131 2.8780	-4198 2.8768	-3206 2.8890	-4570 2.8621	-4687 2.8593	-4520 2.8618	-4280 2.8650	-4503 2.8656
$Ni_{50-y/2}Al_{50-y/2}(Ti,X)_y$								
Ti(Ni)+X(Al)	-4030 2.8860	-4176 2.8849	-3630 2.8901	-4515 2.8681	-4429 2.8675	-4441 2.8672	-4293 2.8708	-4431 2.8719
Ti(Al)+X(Ni)	-5338 2.8720	-5212 2.8733	-3831 2.8892	-5775 2.8569	-6056 2.8527	-5827 2.8559	-5331 2.8612	-5483 2.8624
Ti(Al)Ni+X(Al)	-4642 2.8787	-4974 2.8777	-4630 2.8808	-5187 2.8622	-5019 2.8625	-5033 2.8623	-5046 2.8637	-5138 2.8657
Ti(Al)Ni +X(Ni)Al	-4641 2.8787	-4520 2.8793	-3181 2.8955	-5024 2.8637	-5249 2.8599	-5059 2.8627	-4673 2.8671	-4767 2.8690
Ti(Ni)Al+X(Ni)	-3971 2.8849	-4103 2.8830	-3242 2.8941	-4462 2.8686	-4577 2.8657	-4380 2.8687	-4181 2.8712	-4359 2.8724
Ti(Ni)Al +X(Al)Ni	-3971 2.8849	-3669 2.8893	-3234 2.8939	-4081 2.8721	-4027 2.8711	-4021 2.8711	-3886 2.8745	-3870 2.8773

Table 7 Energies of formation and equilibrium lattice parameter for $Ni_{50}(Al,Ti,X)_{50}$ and for $Ni_{50-y/2}Al_{50-y/2}(Ti,X)_y$ alloys (where the Ni and Al ratio is kept constant at 1:1), for X = Hf, Zr, Ta, Cu, Co, Fe, Cr and Si. The shaded cells indicate the lowest energy state. The shaded cells indicate the lowest energy state for each element. In all cases it is assumed that the Ti and X atoms are located

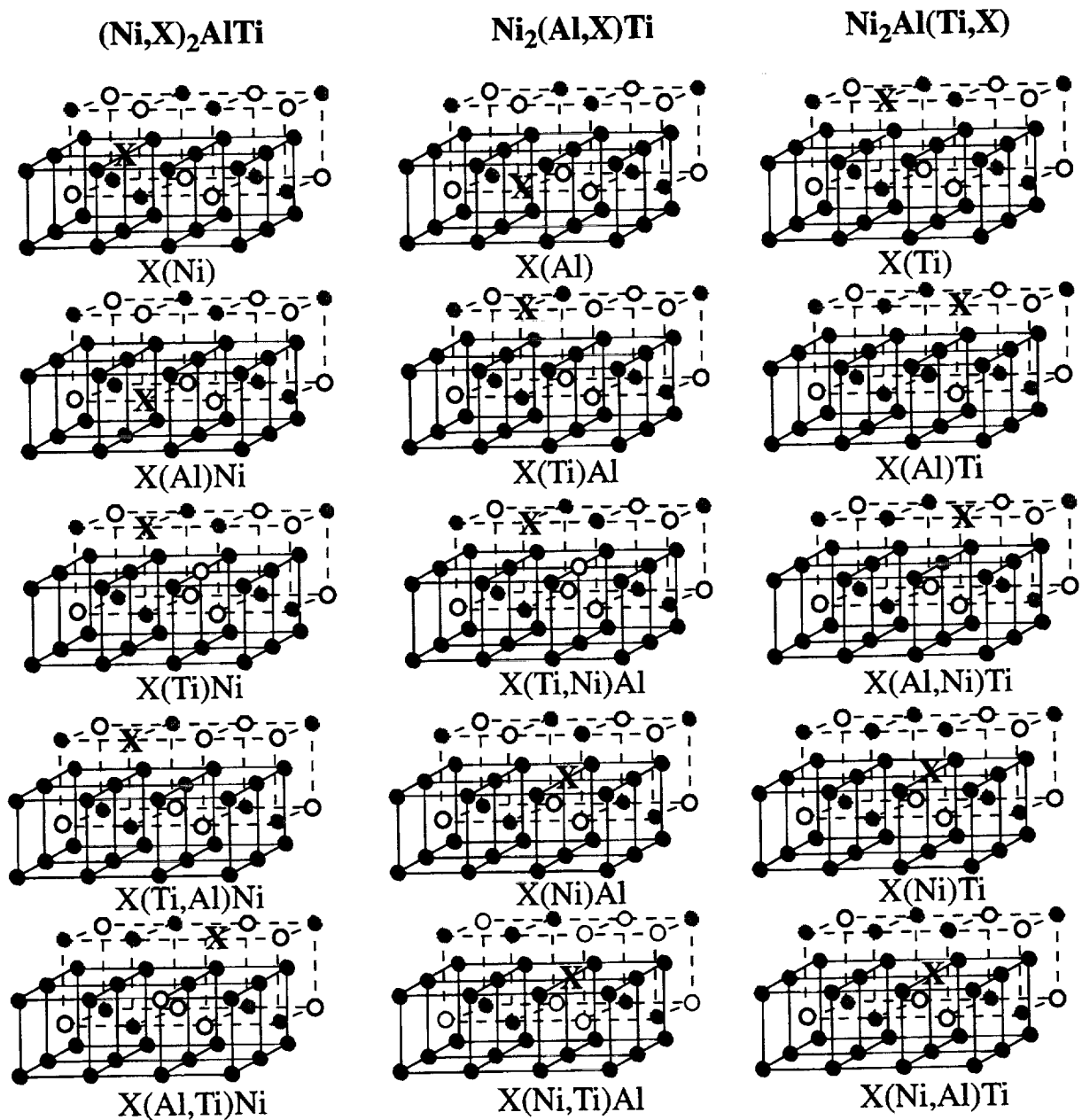


Figure 12: Atomic distributions of X additions to a Ni_2AlTi alloy. Ni-poor, Al-poor and Ti-poor alloys are indicated in each column. Ni, Al and Ti atoms are indicated with solid black disks, solid grey disks and open circles, respectively. The additional element is denoted with the symbol X.

$Ni_2AlTi+X$	Hf	Zr	Ta	Cu	Co	Fe	Cr
--------------	----	----	----	----	----	----	----

$(Ni,X)_2AlTi$

X(Ni)	-0.4122 2.9351	-0.3599 2.9398	-0.2274 2.9540	-0.4422 2.9274	-0.4716 2.9187	-0.4586 2.9199	-0.4122 2.9253
X(Al)Ni	-0.3856 2.9391	-0.4102 2.9373	-0.3757 2.9392	-0.4314 2.9226	-0.4130 2.9230	-0.4144 2.9227	-0.4135 2.9243
X(Ti)Ni	-0.2782 2.9488	-0.3043 2.9467	-0.2845 2.9471	-0.3238 2.9322	-0.3058 2.9324	-0.3077 2.9321	-0.3016 2.9345
X(Ti,Al)Ni	-0.3810 2.9396	-0.4108 2.9372	-0.3859 2.9383	-0.4268 2.9231	-0.4074 2.9235	-0.4089 2.9232	-0.4095 2.9246
X(Al,Ti)Ni	-0.2782 2.9488	-0.3000 2.9472	-0.2731 2.9483	-0.3238 2.9322	-0.3067 2.9324	-0.3084 2.9320	-0.3013 2.9345

$Ni_2(Al,X)Ti$

X(Al)	-0.4497 2.9280	-0.4476 2.9298	-0.4006 2.9323	-0.4564 2.9159	-0.4366 2.9164	-0.4429 2.9154	-0.4381 2.9176
X(Ti)Al	-0.4466 2.9293	-0.4492 2.9296	-0.4098 2.9315	-0.4525 2.9163	-0.4319 2.9169	-0.4384 2.9159	-0.4348 2.9178
X(Ti,Ni)Al	-0.2842 2.9426	-0.3104 2.9405	-0.2897 2.9411	-0.3304 2.9260	-0.3124 2.9263	-0.3143 2.9259	-0.3081 2.9284
X(Ni)Al	-0.4153 2.9294	-0.3522 2.9351	-0.2005 2.9512	-0.4351 2.9176	-0.4647 2.9133	-0.4529 2.9149	-0.4101 2.9194
X(Ni,Ti)Al	-0.4107 2.9298	-0.3508 2.9352	-0.2003 2.9513	-0.4310 2.9180	-0.4596 2.9138	-0.4480 2.9154	-0.4063 2.9198

$Ni_2Al(Ti,X)$

X(Ti)	-0.4538 2.9258	-0.4572 2.9261	-0.4183 2.9275	-0.4598 2.9127	-0.4392 2.9133	-0.4457 2.9123	-0.4423 2.9143
X(Al)Ti	-0.4564 2.9256	-0.4552 2.9262	-0.4089 2.9288	-0.4633 2.9124	-0.4435 2.9129	-0.4499 2.9119	-0.4452 2.9140
X(Al,Ni)Ti	-0.3779 2.9317	-0.4040 2.9297	-0.3720 2.9314	-0.4245 2.9152	-0.4058 2.9156	-0.4073 2.9153	-0.4073 2.9167
X(Ni)Ti	-0.4162 2.9266	-0.3709 2.9306	-0.2282 2.9460	-0.4394 2.9144	-0.4658 2.9104	-0.4520 2.9122	-0.4127 2.9164
X(Ni,Al)Ti	-0.4211 2.9261	-0.3745 2.9303	-0.2281 2.9460	-0.4435 2.9140	-0.4707 2.9099	-0.4569 2.9118	-0.4154 2.9162

Table 8 Hf, Zr, Ta, Cu, Co, Fe and Cr additions to Ni_2AlTi alloys. Energies of formation (in eV/atom) and equilibrium lattice parameter for the atomic configurations displayed in Fig. 12. The dark shaded cells indicate the lowest energy case. The light shaded cells indicate those states that are both close in energy and lattice parameter to the lowest energy state.

$Ni_2AlTi+X$	Nb	Mo	V	W	Ru	Si
--------------	----	----	---	---	----	----

$(Ni,X)_2AlTi$

X(Ni)	-0.2340 2.9524	-0.2580 2.9482	-0.3779 2.9306	-0.2383 2.9516	-0.4720 2.9261	-0.3639 2.9324
X(Al)Ni	-0.3915 2.9367	-0.3953 2.9359	-0.4224 2.9265	-0.3892 2.9379	-0.4311 2.9287	-0.4232 2.9265
X(Ti)Ni	-0.2981 2.9449	-0.2962 2.9445	-0.3059 2.9370	-0.2955 2.9460	-0.2924 2.9425	-0.3301 2.9346
X(Ti,Al)Ni	-0.3978 2.9361	-0.3953 2.9359	-0.4178 2.9269	-0.3929 2.9375	-0.4286 2.9287	-0.4235 2.9264
X(Al,Ti)Ni	-0.2891 2.9457	-0.2924 2.9449	-0.3068 2.9369	-0.2885 2.9466	-0.2930 2.9425	-0.3298 2.9346

$Ni_2(Al,X)Ti$

X(Al)	-0.4212 2.9294	-0.4225 2.9291	-0.4477 2.9198	-0.4221 2.9304	-0.4529 2.9224	-0.4639 2.9181
X(Ti)Al	-0.4273 2.9288	-0.4221 2.9292	-0.4433 2.9202	-0.4254 2.9301	-0.4516 2.9223	-0.4614 2.9184
X(Ti,Ni)Al	-0.3036 2.9388	-0.3019 2.9385	-0.3123 2.9308	-0.3011 2.9400	-0.2982 2.9365	-0.3373 2.9283
X(Ni)Al	-0.2260 2.9476	-0.2434 2.9449	-0.3825 2.9247	-0.2237 2.9480	-0.4632 2.9217	-0.3561 2.9277
X(Ni,Ti)Al	-0.2254 2.9477	-0.2417 2.9451	-0.3776 2.9252	-0.2227 2.9481	-0.4576 2.9222	-0.3555 2.9277

$Ni_2Al(Ti,X)$

X(Ti)	-0.4354 2.9253	-0.4291 2.9258	-0.4505 2.9167	-0.4330 2.9267	-0.4594 2.9188	-0.4689 2.9148
X(Al)Ti	-0.4289 2.9259	-0.4289 2.9258	-0.4543 2.9164	-0.4292 2.9270	-0.4602 2.9189	-0.4710 2.9146
X(Al,Ni)Ti	-0.3878 2.9289	-0.3904 2.9284	-0.4169 2.9189	-0.3854 2.9303	-0.4243 2.9213	-0.4172 2.9189
X(Ni)Ti	-0.2511 2.9426	-0.2602 2.9407	-0.3733 2.9229	-0.2465 2.9433	-0.4616 2.9190	-0.3809 2.9226
X(Ni,Al)Ti	-0.2509 2.9426	-0.26000 2.9407	-0.3741 2.9228	-0.2459 2.9434	-0.4653 2.9186	-0.3851 2.9221

Table 8 (continued) Nb, Mo, V, W, Ru and Si additions to Ni_2AlTi alloys. Energies of formation (in eV/atom) and equilibrium lattice parameter for the atomic configurations displayed in Fig. 12. The shaded cells indicate the lowest energy case. The dotted cells indicate those states that are both close in energy and lattice parameter to the ground state ones.

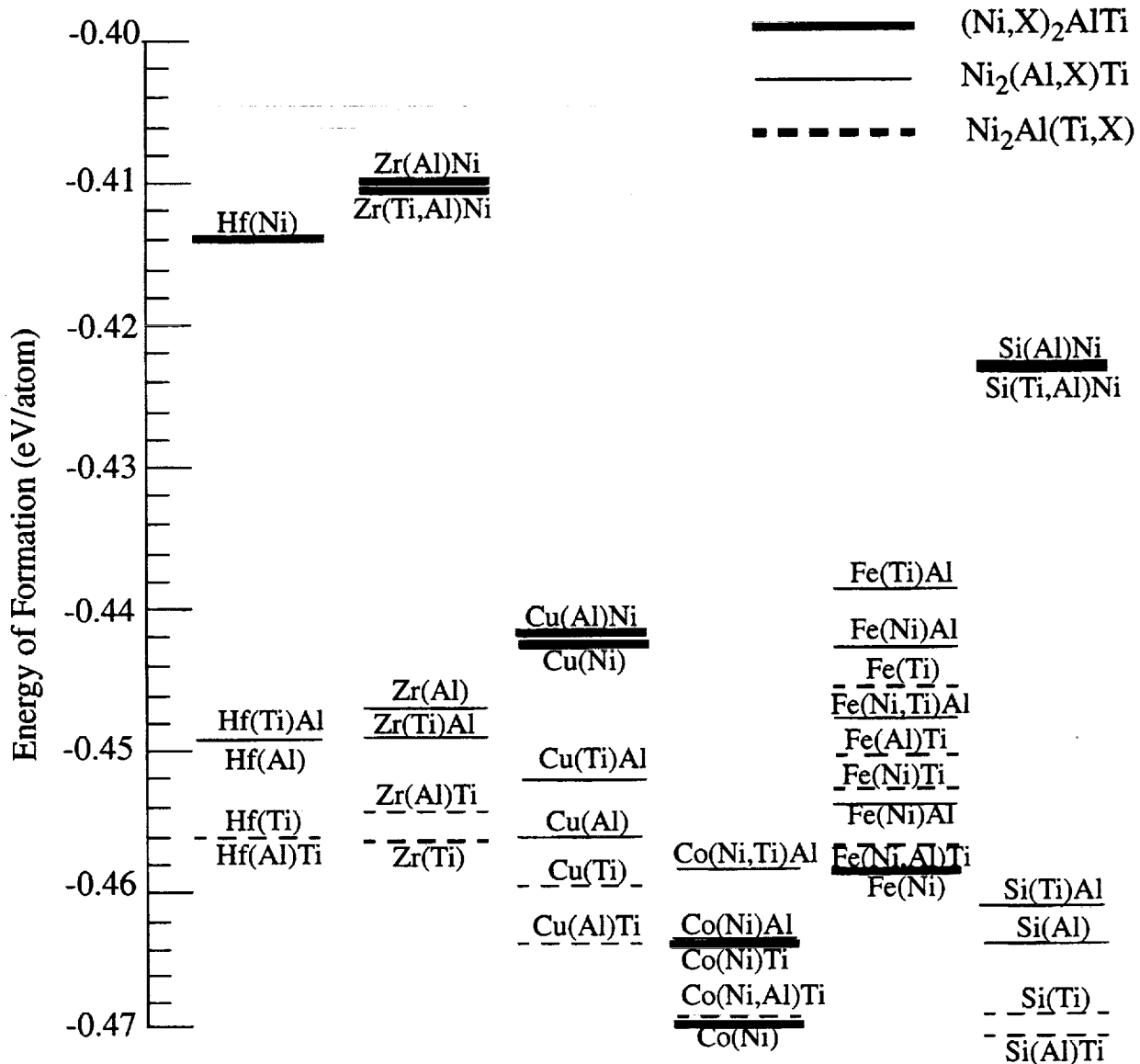


Figure 13: Energy of formation (in eV/atom) for the Heusler alloys shown in Fig. 12 for Hf, Zr,

For such a complex system, the energy spectrum introduced in previous sections becomes perhaps the only way to investigate the trends exhibited by these systems. The energy spectrum corresponding to these numerical results is shown in Fig. 13. In spite of the similarities with the ternary case, it should be noted that the bonding scheme in the Heusler phase is quite different than that found in NiAl alloys. Fig. 13 shows that while Zr, Hf, Cu and Si show a distinct preference for the sublattice occupied by Ti and Al atoms, there seems to be a low energy price to pay

for substitutions in Al or Ti sites, even at the expense of an antistructure defect created when Ti goes to an Al site in the X(Ti)Al cases. A clear distinction is seen for Co and Fe, where both show a marked preference for Ni sites.

A complete presentation of the BFS results for all possible additions to all the Heusler alloys which can be obtained from the 16 elements considered in this work is, as mentioned above, beyond the scope of this paper, but not the computational method. We therefore limit our comments on such systems to the Ni₂AlTi +X case (Table 7, Figs. 12-13) and to providing approximate expressions using the BF rule (6) for the changes in lattice parameter for alloying additions in the dilute limit for general Heusler alloys (A₂BC)_{1-x}X_x,

$$\frac{a(x)}{a_H} = 1 + \mu x \quad (17)$$

with

$$\mu = \frac{\gamma_X - \gamma_i}{\gamma_H} - \frac{\lambda_X - \lambda_i}{\lambda_H} \quad (18)$$

where $\gamma_i = B_i a_i^2$, $\lambda_i = B_i a_i$, for $i = A, B, C$ or X , and where γ_H and λ_H are given by

$$\gamma_H = \frac{2\gamma_A + \gamma_B + \gamma_C}{4} \quad (19)$$

and

$$\lambda_H = \frac{2\lambda_A + \lambda_B + \lambda_C}{4}. \quad (20)$$

Several intermetallics of potential industrial interest form Heusler precipitates for small levels of additions. Some alloying additions, like Hf, Zr, Ta or Nb in NiAl, have a low solubility limit and result in the precipitation of Heusler particles. Such effect was studied in detail for the case of Ti in NiAl (10), where BFS was applied to the determination of the solubility limit of Ti in NiAl

and second phase formation. It is then important to examine the role of other additions and to determine, beyond their site preference in either phase (in the case of two phase alloys), their partitioning behavior.

The current formalism can be easily extended to provide similar information for the large family of alloys that exhibit the Heusler structure (Ni_2AlX , with $X = \text{Nb, Ta, Hf, Zr}$; Co_2AlX , $X = \text{Nb, Ta, Hf, Zr}$ and Ti ; Cu_2AlX , $X = \text{Hf, Zr}$; and Fe_2AlX , $X = \text{V, Cr, Co, Ni}$). In addition, as noted for the case of binary systems, there are no restrictions in the formalism for the number of simultaneous alloying additions considered in the base alloy. Natural extensions of this work to high order additions in binary and ternary ordered intermetallics as well as other base systems (Ni_3Al , Ni-base superalloys, etc.) are also being performed.

Conclusions

The BFS method was used to determine the site preference scheme for a large number of alloying additions to NiAl , FeAl and CoAl . A detailed analysis of all the possible site substitutions was performed enhancing our understanding of the interrelationship between multiple alloying additions. Because the agreement with experiment was excellent in all cases, the analysis was extended to ternary (Heusler) alloys where no data on the effect of alloying additions on structure exist.

Acknowledgments

Frutiful discussions with N. Bozzolo are gratefully acknowledged. We would also like to thank C. Amador for providing us with the first-principles input necessary for determining the BFS parameters used in this work.

References

1. G. Bozzolo and J. Ferrante, *J. Computer-Aided Mater. Design* 2 (1995), 113, and references therein; G. Bozzolo and J. Ferrante, *Ultramicroscopy* 42/44 (1992), 55; G. Bozzolo, R. Ibanez-Meier and J. Ferrante, *Mat. Res. Soc. Symp. Proc.* 355 (1995), 531.

2. P. H. Kitabjian, A. Garg, R. D. Noebe and W. D. Nix, *Creep and Fracture of Engineering Materials and Structures*, (The Minerals, Metals & Materials Society, Warrendale, PA 1997), pp. 667.
3. R. D. Noebe and W. S. Walston, *Structural Intermetallics 1997* (The Minerals, Metals & Materials Society, Warrendale, PA, 1997), pp. 573.
4. G. Bozzolo, J. Ferrante, R. D. Noebe and C. Amador, *Scripta Mater.* 33 (1995), 1907.
5. G. Bozzolo, J. Ferrante, R. D. Noebe and C. Amador, *Scripta Mater.* 36 (1997), 813.
6. G. Bozzolo and J. Ferrante, *Phys. Rev. B* 50 (1994), 5971.
7. G. Bozzolo, J. Ferrante and A. M. Rodriguez, *J. Computer-Aided Mater. Design* 1 (1993), 285.
8. J. H. Rose, J. R. Smith and J. Ferrante, *Phys. Rev. B* 28 (1983) 1835.
9. O. K. Andersen, A. V. Postnikov and S. Y. Savrasov, *Mat. Res. Soc. Symp. Proc.* 253 (1992), 37.
10. G. Bozzolo, R. D. Noebe, J. Ferrante and A. Garg, *Structural Intermetallics 1997* (The Minerals, Metals and Materials Society, 1997), pp. 665.
11. N. V. Allaverdoba, V. K. Portnoy, L. A. Kucherenko, A. V. Ruban and V. I. Bogdanov, *J. Less-Common Metals* 141 (1988), 191.
12. D. J. Chakrabarti, *Met. Trans.* 8 (1977) 121; O. S. Zarechnyuk, N. V. German, T. I. Yanson, R. M. Rykhal and A. A. Muravieva, *Phase Equilibria in Metals and Alloys* (Nauka, Moscow, 1981), pp. 69.
13. C. L. Fu and J. Zou, *Acta Mater.* 44 (1996), 1471.
14. C. R. Kao, L. M. Pike, S. -L. Chen and Y. A. Chang, *Intermetallics* 2 (1994), 235.
15. H. Hosoda, K. Inoue and Y. Mishima, *Mat. Res. Soc. Symp. Proc.* 364 (1995), 437.
16. I. M. Anderson, A. J. Duncan and J. Bentley, *Mat. Res. Soc. Symp. Proc.* 364 (1995), 443.
17. P. Chartier, M. Balasubramanian, D. Brewster, T. Manzur, D. Pease, J. Budnick, L. Huang, C. Law, S. Russel and C. Kimball, *J. Appl. Phys.* 75 (1994), 3842.
18. A. J. Duncan, M. J. Kaufman, C. T. Liu and M. K. Miller, *Appl. Surf. Sci.* 76/77 (1994), 155.
19. R. D. Field, D. F. Lahrman, R. Darolia, *Acta Metall. Mater.* 39 (1991), 2961.
20. J. D. Cotton, R. D. Noebe, M. J. Kaufman, *Intermetallics* 1 (1993), 1.
21. P. R. Munroe and I. Baker, *J. Mater. Res.* 7 (1992), 2119.
22. S. Khosla, (PhD Thesis, University of Knoxville, TN, 1993).
23. I. M. Anderson, *Acta Mater.* 45 (1997), 3897.

REPORT DOCUMENTATION PAGE			Form Approved OMB No. 0704-0188	
Public reporting burden for this collection of information is estimated to average 1 hour per response, including the time for reviewing instructions, searching existing data sources, gathering and maintaining the data needed, and completing and reviewing the collection of information. Send comments regarding this burden estimate or any other aspect of this collection of information, including suggestions for reducing this burden, to Washington Headquarters Services, Directorate for Information Operations and Reports, 1215 Jefferson Davis Highway, Suite 1204, Arlington, VA 22202-4302, and to the Office of Management and Budget, Paperwork Reduction Project (0704-0188), Washington, DC 20503.				
1. AGENCY USE ONLY (Leave blank)	2. REPORT DATE October 1998	3. REPORT TYPE AND DATES COVERED Technical Memorandum		
4. TITLE AND SUBTITLE Modeling of Substitutional Site Preference in Ordered Intermetallic Alloys			5. FUNDING NUMBERS WU-523-22-13-00	
6. AUTHOR(S) Guillermo Bozzolo, Ronald D. Noebe, and Frank Honeyc				
7. PERFORMING ORGANIZATION NAME(S) AND ADDRESS(ES) National Aeronautics and Space Administration Lewis Research Center Cleveland, Ohio 44135-3191			8. PERFORMING ORGANIZATION REPORT NUMBER E-11387	
9. SPONSORING/MONITORING AGENCY NAME(S) AND ADDRESS(ES) National Aeronautics and Space Administration Washington, DC 20546-0001			10. SPONSORING/MONITORING AGENCY REPORT NUMBER NASA TM-1998-208665	
11. SUPPLEMENTARY NOTES Prepared for the "Interstitial and Substitutional Effects in Intermetallics" Fall Meeting sponsored by the Minerals, Metals, and Materials Society, Rosemont, Illinois, October 11-15, 1998. Guillermo Bozzolo, Ohio Aerospace Institute, 22800 Cedar Point Road, Cleveland, Ohio 44142; Ronald D. Noebe and Frank Honeyc, NASA Lewis Research Center. Responsible person, Guillermo Bozzolo, organization code 5140, (216) 433-5824.				
12a. DISTRIBUTION/AVAILABILITY STATEMENT Unclassified - Unlimited Subject Category: 26 This publication is available from the NASA Center for AeroSpace Information, (301) 621-0390.			12b. DISTRIBUTION CODE Distribution: Nonstandard	
13. ABSTRACT (Maximum 200 words) We investigate the site substitution scheme of specific alloying elements in ordered compounds and the dependence of site occupancy on compound stoichiometry, alloy concentration. This basic knowledge, and the interactions with other alloying additions are necessary in order to predict and understand the effect of various alloying schemes on the physical properties of a material, its response to various temperature treatments, and the resulting mechanical properties. Many theoretical methods can provide useful but limited insight in this area, since most techniques suffer from constraints in the type of elements and the crystallographic structures that can be modeled. With this in mind, the Bozzolo-Ferrante-Smith (BFS) method for alloys was designed to overcome these limitations, with the intent of providing a useful tool for the theoretical prediction of fundamental properties and structure of complex systems. After a brief description of the BFS method, its use for the determination of site substitution schemes for individual as well as collective alloying additions to intermetallic systems is described, including results for the concentration dependence of the lattice parameter. Focusing on B2 NiAl, FeAl and CoAl alloys, the energetics of Si, Ti, V, Cr, Fe, Co, Ni, Cu, Zr, Nb, Mo, Ru, Hf, Ta and W alloying additions are surveyed. The effect of single additions as well as the result of two simultaneous additions, discussing the interaction between additions and their influence on site preference schemes is considered. Finally, the BFS analysis is extended to ternary L ₁₂ (Heusler phase) alloys. A comparison between experimental and theoretical results for the limited number of cases for which experimental data is available is also included.				
14. SUBJECT TERMS Intermetallics; Monte Carlo; Atomistic simulations; BFS; Alloy; Semiempirical			15. NUMBER OF PAGES 43	
			16. PRICE CODE A03	
17. SECURITY CLASSIFICATION OF REPORT Unclassified	18. SECURITY CLASSIFICATION OF THIS PAGE Unclassified	19. SECURITY CLASSIFICATION OF ABSTRACT Unclassified	20. LIMITATION OF ABSTRACT	